HHS Public Access

Author manuscript

Nat Immunol. Author manuscript; available in PMC 2019 November 06.

Published in final edited form as:

Nat Immunol. 2019 June ; 20(6): 687–700. doi:10.1038/s41590-019-0382-5.

Bhlhe40 mediates tissue-specific control of macrophage proliferation in homeostasis and type 2 immunity

Nicholas N. Jarjour[1], **Elizabeth A. Schwarzkopf**[1], **Tara R. Bradstreet**[1], **Irina Shchukina**[1], **Chih-Chung Lin**[1,4], **Stanley Ching-Cheng Huang**[1,5], **Chin-Wen Lai**[1], **Melissa E. Cook**[1], **Reshma Taneja**[2], **Thaddeus S. Stappenbeck**[1], **Gwendalyn J. Randolph**[1], **Maxim N. Artyomov**[1], **Joseph F. Urban Jr.**[3], and **Brian T. Edelson**[1,*]

[1]Department of Pathology and Immunology, Washington University School of Medicine, St. Louis, MO 63110

[2]Department of Physiology, Yong Loo Lin School of Medicine, National University of Singapore, Singapore 117597

[3]United States Department of Agriculture (USDA), Agriculture Research Service, Beltsville Human Nutrition Research Center, Diet, Genomics, and Immunology Laboratory, Beltsville, MD 20705

[4]Present address: Department of Neurology, Massachusetts General Hospital and Harvard Medical School, Charlestown, MA 02129

[5]Present address: Department of Pathology, Case Western Reserve University School of Medicine, Cleveland, OH 44106

Abstract

Most tissue-resident macrophage populations develop during embryogenesis, self-renew in the steady-state and expand during type 2 immunity. Whether shared mechanisms regulate the proliferation of macrophages in homeostasis and disease is unclear. Here we found that the transcription factor Bhlhe40 was required in a cell-intrinsic manner for the self-renewal and maintenance of large peritoneal macrophages (LPMs), but not that of other tissue-resident macrophages. Bhlhe40 was necessary for the proliferation, but not the polarization, of LPMs in response to the cytokine IL-4. During infection with the helminth *Heligmosomoides polygyrus bakeri*, Bhlhe40 was required for cell cycling of LPMs. Bhlhe40 repressed the expression of genes encoding the transcription factors c-Maf and Mafb and directly promoted expression of transcripts encoding cell cycle-related proteins to enable the proliferation of LPMs. In LPMs, Bhlhe40 bound to genomic sites co-bound by the macrophage lineage-determining factor PU.1 and to unique sites,

*Corresponding Author: Brian T. Edelson; bedelson@path.wustl.edu.

Author Contributions

N.N.J designed, performed and analyzed experiments and wrote the manuscript. E.A.S., T.R.B., C.-C.L., M.E.C. and C.-W. L. performed experiments. S.C.-C.H. provided reagents, protocols and technical expertise. I.S. and M.N.A. analyzed ChIP-seq data. R.T. provided mice. T.S.S., G.J.R. and J.F.U. provided reagents and technical expertise. B.T.E. designed and analyzed experiments, supervised the studies, and wrote the manuscript.

Competing Interests

The authors declare no competing financial interests.

including *Maf* and loci encoding cell cycle-related proteins. Our findings demonstrate a tissue-specific control mechanism that regulates the proliferation of resident macrophages in homeostasis and type 2 immunity.

Tissue-resident macrophages are established during embryogenesis[1,2,3] and are largely maintained by local self-renewal within each organ[4,5]. While some transcription factors specifying distinct macrophage lineages have been described[3], differences in the transcriptional basis for self-renewal in distinct macrophage populations are not well understood. Established regulators of self-renewal in multiple macrophage lineages include the anti-proliferative transcription factors c-Maf and MafB[6,7], as well as the pro-proliferative deacetylase Sirtuin1[8]. The transcription factor GATA6 may exercise tissue-specific control of macrophage self-renewal, as loss of GATA6 causes large peritoneal macrophages (LPMs) to become multinucleated and impairs their proliferation[9]. However, deletion of GATA6 also causes changes in the morphology, surface markers and gene expression profile of LPMs[9,10,11], illustrating that the study of tissue-specific control of resident macrophage self-renewal can be confounded by significant effects on macrophage identity. It remains unclear to what extent macrophage self-renewal is regulated in a tissue-specific manner and whether any tissue-specific regulation that does exist cooperates with broadly shared regulators.

In addition to their homeostatic self-renewal capacity, resident macrophages can become alternatively activated in response to type 2 cytokines produced in response to stimuli like helminth infection, resulting in dramatic proliferation concomitant with acquisition of a pro-repair or anti-helminth protein expression profile[12,13,14,15]. Until recently, proliferation of all macrophages elicited by type 2 immunity was assumed to be controlled by cytokine signaling through JAK kinases and STAT transcription factors. While it remains unclear whether tissue-specific, cell-intrinsic transcriptional regulation influences this process, the collagens SP-A and C1q act through the receptor Myo18a to mediate extrinsic, tissue-specific regulation of proliferation and alternative activation[15]. Signaling through receptors for apoptotic cells also influences these processes in tissue-resident macrophages[16]. Furthermore, differences in alternative activation between monocyte-derived and resident macrophages indicate that ontogeny influences responses during type 2 immunity[17,18]. Whether there are common regulators of macrophage self-renewal at steady-state and proliferation during disease remains unknown.

The transcription factor Bhlhe40 is expressed in some hematopoietic and non-hematopoietic cell types[19,20], including select resident macrophage populations[21]. Bhlhe40 binds to DNA at class B E-box motifs and functions primarily as a transcriptional repressor[22,23], although examples of transcriptional activation have been described[24,25]. Bhlhe40 is dysregulated in some cancers and may regulate cell cycling in specific contexts[20]. A variety of hematopoietic cell types are regulated by Bhlhe40, including NKT cells and B cells[26,27,28,29], and it controls cytokine production in T cells during infection and autoimmunity[21,30,31,32,33]. Bhlhe40 and c-Maf may be interconnected in the regulation of the cytokine IL-10, but how this would occur is unclear[32,34]. Despite an emerging view that Bhlhe40 is an important regulator of immunity, little is known regarding its role in myeloid

cells. Bhlhe40 has been proposed as a tissue-specific binding partner of PU.1 in LPMs, but this has not been directly tested[35].

Here we found that Bhlhe40 had a unique and cell-intrinsic role in LPMs to regulate self-renewal, proliferation and accumulation during type 2 immunity. In LPMs, Bhlhe40 bound a subset of genomic sites bound by the macrophage lineage-specifying transcription factor PU.1, but also many unique sites, including loci encoding cell cycle-related proteins such as c-Maf. Loss of Bhlhe40 in LPMs led to higher expression of *Maf* and *Mafb* mRNA and lower expression of cell cycle-related transcripts. Our findings establish Bhlhe40 as a tissue-specific transcriptional regulator of LPM proliferation active in both homeostatic self-renewal and upon rapid cell cycling during type 2 immunity.

Results

Loss of Bhlhe40 selectively reduces LPMs

Because Bhlhe40 expression has been observed in select resident macrophage populations[21,36,37], we examined macrophages from mice transgenic for a *Bhlhe40*^{GFP} bacterial artificial chromosome (*Bhlhe40*$^{GFP+}$ mice hereafter)[21]. We observed low or undetectable GFP expression in Ly6G^{-}CD115^{+} Ly6C^{hi} and Ly6C^{lo} blood monocytes, F4/80^{hi} splenic red pulp macrophages (hereafter red pulp macrophages), CD45^{int}CD11b^{+} central nervous system microglia, CD45^{+}CD11b^{lo}F4/80^{hi} liver Kupffer cells (hereafter Kupffer cells), CD45^{+}Ly6C^{-}CD11b^{+}F4/80^{hi} kidney macrophages (hereafter kidney macrophages) and CD45^{+}Ly6C^{-}F4/80^{+}CD64^{+}MHC-II^{+} small intestinal lamina propria macrophages (hereafter SI macrophages), but found high expression of GFP in CD45^{+}Siglec-F^{+}CD11c^{+} lung alveolar macrophages (hereafter AMs), CD115^{+}CD11b^{+}ICAM2^{+}MHC-II^{int} large peritoneal macrophages (hereafter LPMs), CD115^{+}CD11b^{+}MHC-II^{+}ICAM2^{-} small peritoneal macrophages (hereafter SPMs), CD115^{+}CD11b^{+}ICAM2^{+}MHC-II^{int} large pleural macrophages (hereafter large pleural macrophages) and CD115^{+}CD11b^{+}MHC-II^{+}ICAM2^{-} small pleural macrophages (hereafter small pleural macrophages) (Fig. 1a and Supplementary Fig. 1). Of the populations examined, only LPMs and SPMs were decreased in *Bhlhe40*$^{-/-}$ compared to *Bhlhe40*$^{+/+}$ mice (Fig. 1b,c and Supplementary Fig. 1). In some resident macrophage populations, including LPMs, Tim4 is a marker of embryonically-derived, long-lived resident macrophages[38,39,40], while CD226 marks mature SPMs[41]. Decreases in Tim4^{+} LPMs and CD226^{+} SPMs largely accounted for the reduced number of peritoneal macrophages in *Bhlhe40*$^{-/-}$ mice (Supplementary Fig. 1). The number of peritoneal CD115^{-}MHC-II^{+}CD19^{+} B cells (hereafter B cells) was not reduced in *Bhlhe40*$^{-/-}$ compared to *Bhlhe40*$^{+/+}$ mice (Supplementary Fig. 1). Therefore, loss of Bhlhe40 selectively reduced the number of LPMs and SPMs.

Bhlhe40 is required in LPMs for self-renewal

To address whether the loss of LPMs in *Bhlhe40*$^{-/-}$ mice was due to impaired proliferation, we stained peritoneal cells from *Bhlhe40*$^{+/+}$ and *Bhlhe40*$^{-/-}$ mice for Ki67, a marker of cycling cells. We observed a 4-fold increase in the frequency of Ki67^{+} LPMs (Fig. 1d,e), but little change in the frequency of Ki67^{+} SPMs and peritoneal B cells in *Bhlhe40*$^{-/-}$ compared to *Bhlhe40*$^{+/+}$ mice (Fig. 1e). Despite normal numbers, we found an increase in the

frequency of Ki67^{+} large pleural macrophages in *Bhlhe40*$^{-/-}$ compared to *Bhlhe40*$^{+/+}$ mice (Supplementary Fig. 1). There was no difference in the uptake of bromodeoxyuridine (BrdU), which is incorporated during the S phase, in LPMs from *Bhlhe40*$^{+/+}$ and *Bhlhe40*$^{-/-}$ mice 3 hours after injection with BrdU (Fig. 1f,g). Staining for the mitosis marker phosphohistone H3 (pHH3) was similar in *Bhlhe40*$^{+/+}$ and *Bhlhe40*$^{-/-}$ LPMs (Fig. 1h,i). When using Ki67 and the nuclear stain 4′,6-diamidino-2-phenylindole (DAPI) to separate the phases of the cell cycle, we observed an increased number of LPMs in the G1 phase (Fig. 1j,k), but similar numbers of LPMs in the S, G2 and M phases in *Bhlhe40*$^{-/-}$ compared to *Bhlhe40*$^{+/+}$ mice (Fig. 1j,k), suggesting that *Bhlhe40*$^{-/-}$ LPMs were impaired in progressing from G1, but proliferated sufficiently to maintain a stable, although reduced, population of LPMs. The proportion of LPMs staining for the viability dye 7-aminoactinomycin D (7-AAD) was similar in *Bhlhe40*$^{+/+}$ and *Bhlhe40*$^{-/-}$ mice (Supplementary Fig. 1). Taken together, these data indicate that Bhlhe40 was required for normal proliferation of LPMs.

Bhlhe40 is required intrinsically in LPMs for cell cycling

To address whether the role of Bhlhe40 in LPMs was cell-intrinsic, we generated mixed bone marrow chimeras by co-transfer of equal numbers of *Bhlhe40*$^{+/+}$ (CD45.1) plus either *Bhlhe40*$^{+/+}$ (CD45.2) or *Bhlhe40*$^{-/-}$ (CD45.2) total bone marrow cells into irradiated *Bhlhe40*$^{+/+}$ CD45.1/CD45.2 mice, which were allowed to reconstitute for >8 weeks. Out of peritoneal, blood, splenic, liver, kidney, SI lamina propria, lung and pleural hematopoietic populations examined, only LPMs and large pleural macrophages exhibited Bhlhe40-dependent reconstitution (*Bhlhe40*$^{+/+}$ outnumbering *Bhlhe40*$^{-/-}$ cells by more than 10:1) (Fig. 2a–d, Supplementary Fig. 2 and data not shown). The small number of *Bhlhe40*$^{-/-}$ LPMs in mixed chimeras accumulated in the G1 phase (Fig. 2e,f), indicating that the alterations in cell cycling in *Bhlhe40*$^{-/-}$ LPMs were cell-intrinsic. Next, we bred *LysM-Cre*$^{+}$ *Bhlhe40*$^{fl/fl}$ mice to delete Bhlhe40 in myeloid cells. Compared to *LysM-Cre*$^{-}$ *Bhlhe40*$^{fl/fl}$ mice, *LysM-Cre*$^{+}$ *Bhlhe40*$^{fl/fl}$ mice had a nearly 2-fold reduction in the number of LPMs, with no change in SPMs or peritoneal B cells (Fig. 2g) and an increased proportion of LPMs in the G1 phase (Fig. 2h,i). Finally, we co-transferred *Bhlhe40*$^{+/+}$ (CD45.1) plus either *Bhlhe40*$^{+/+}$ (CD45.2) or *Bhlhe40*$^{-/-}$ (CD45.2) bulk peritoneal cells into resting *Bhlhe40*$^{+/+}$ (CD45.1/CD45.2) mice at ratios calculated to result in the transfer of equal numbers of LPMs (200,000–300,000) from each donor. Over four weeks, the relative proportion of transferred *Bhlhe40*$^{+/+}$ (CD45.1) to *Bhlhe40*$^{-/-}$ (CD45.2) LPMs was increased (Fig. 2j,k and Supplementary Fig. 2), while the relative proportion of transferred *Bhlhe40*$^{+/+}$ (CD45.1) to transferred *Bhlhe40*$^{-/-}$ (CD45.2) B cells was maintained in the peritoneum (Fig. 2j,l and Supplementary Fig. 2), supporting a cell-intrinsic role for Bhlhe40 in mature LPMs. Thus, Bhlhe40 was cell-intrinsically required in LPMs for normal proliferation and maintenance.

Loss of Bhlhe40 dysregulates a unique set of genes in LPMs

Next, we performed gene expression microarrays to determine the transcriptional differences between LPMs from *Bhlhe40*$^{+/+}$ and *Bhlhe40*$^{-/-}$ mice. 84 genes were dysregulated by 2-fold or more in *Bhlhe40*$^{-/-}$ compared to *Bhlhe40*$^{+/+}$ LPMs (Fig. 3a), including expression changes in several genes related to macrophage alternative activation, such as *Chil3*, *Clec10a*, *Mrc1* and *Arg1* (Fig. 3b). We validated these data by flow cytometry for several

proteins encoded by differentially expressed genes (*Emb*, *Clec10a*, *Lyve1*) (Fig. 3c–e). When we assessed the expression of gene ontology sets[42] in the absence of Bhlhe40 using the list of genes that were differentially expressed ≥1.5-fold between *Bhlhe40*$^{+/+}$ and *Bhlhe40*$^{-/-}$ LPMs, we found that the Regulation of cell proliferation gene set was enriched in *Bhlhe40*$^{+/+}$ LPMs, while some immune response-related gene sets were enriched in *Bhlhe40*$^{-/-}$ LPMs (Fig. 3f,g). We validated higher expression of *Maf* and *Mafb* mRNA in *Bhlhe40*$^{-/-}$ compared to *Bhlhe40*$^{+/+}$ LPMs in our microarrays (data not shown) by qRT-PCR (Fig. 3h), consistent with impaired proliferation of *Bhlhe40*$^{-/-}$ LPMs.

Because the transcription factor GATA6 is an important regulator of LPMs[9,10,11], we reanalyzed our microarray data and published microarray data[11] from *LysM-Cre*$^{-}$ *Gata6*$^{fl/fl}$ and *LysM-Cre*$^{+}$ *Gata6*$^{fl/fl}$ LPMs to look for differentially expressed genes regulated by both transcription factors. Expression of *Gata6* mRNA was not substantially changed in *Bhlhe40*$^{-/-}$ LPMs ($\log_2$ expression, *Bhlhe40*$^{+/+}$ 10.24, *Bhlhe40*$^{-/-}$ 10.10; data not shown), nor did loss of GATA6 cause substantial changes in the expression of *Bhlhe40* in LPMs ($\log_2$ expression, *LysM-Cre*$^{-}$ *Gata6*$^{fl/fl}$ 10.04, *LysM-Cre*$^{+}$ *Gata6*$^{fl/fl}$ 9.81; data not shown). Furthermore, the majority of Bhlhe40-dependent genes were not dependent on GATA6 and the converse was likewise true (Supplementary Fig. 2).

Next, we performed transcriptome analysis of AMs, which have high expression of *Bhlhe40*, from *Bhlhe40*$^{+/+}$ and *Bhlhe40*$^{-/-}$ mice. Compared to LPMs, Bhlhe40 controlled a largely distinct and smaller group of genes in AMs, mostly encoding proteins involved in antigen presentation by MHC class II (*H2-Aa*, *H2-Ab1*, *H2-Eb1*, *Cd74*; Fig. 3i). A set of genes selectively expressed in LPMs relative to AMs, splenic red pulp macrophages and microglia has been previously curated[36]. Bhlhe40 regulated the expression of only a small subset of these genes (*Lrg1*, *Stard13*, *Nedd4*) (Supplementary Fig. 2). Therefore, Bhlhe40 regulated a cell type-specific set of genes in LPMs, but was dispensable for identity.

Bhlhe40 is required for LPM responses during type 2 immunity

We then asked whether Bhlhe40 was required for macrophage accumulation during peritoneal immune responses characterized either by the differentiation of monocyte-derived macrophages or the local proliferation of LPMs. Intraperitoneal (i.p.) injection of thioglycollate, which elicits the recruitment and differentiation of blood-derived monocytes to the peritoneum independent of proliferation[17,43], resulted in equivalent accumulation of CD115^{+}CD11b^{+}ICAM2^{lo} thioglycollate-elicited macrophages (hereafter thioglycollate-elicited macrophages) in *Bhlhe40*$^{+/+}$ and *Bhlhe40*$^{-/-}$ mice after 4 days (Fig. 4a,b), while the i.p injection of IL-4+anti-IL-4 antibody complexes (hereafter IL-4c), which elicit the robust proliferation of resident macrophages[12], caused a 5-fold increase in the number of LPMs in *Bhlhe40*$^{+/+}$ mice compared to *Bhlhe40*$^{-/-}$ mice after 4 days (Fig. 4c,d). Similar findings were obtained in *LysM-Cre*$^{-}$ *Bhlhe40*$^{fl/fl}$ and *LysM-Cre*$^{+}$ *Bhlhe40*$^{fl/fl}$ mice (Fig. 4d), suggesting Bhlhe40 was required for the proliferation of resident LPMs in a cell-intrinsic manner. SPMs were not reduced in *Bhlhe40*$^{-/-}$ and *LysM-Cre*$^{+}$ *Bhlhe40*$^{fl/fl}$ compared to *Bhlhe40*$^{+/+}$ and *LysM-Cre*$^{-}$ *Bhlhe40*$^{fl/fl}$ mice in response to IL-4c (Fig. 4e). Because Bhlhe40 represses the production of IL-10 in T cells and myeloid cells[21,31,32,33], we injected IL-4c i.p. into *Bhlhe40*$^{-/-}$ *Il10*$^{-/-}$ mice to test whether lack of IL-10 restored the IL-4c-

driven accumulation of LPMs in the absence of Bhlhe40. Similar to *Bhlhe40*$^{-/-}$ mice, *Bhlhe40*$^{-/-}$ *Il10*$^{-/-}$ mice had poor accumulation of LPMs after injection of IL-4c (Supplementary Fig. 3), indicating IL-10 did not contribute to the impaired response of *Bhlhe40*$^{-/-}$ LPMs. Taken together, these data indicate that Bhlhe40 was required for normal accumulation of LPMs in response to IL-4c.

Bhlhe40 regulates proliferation, but not polarization, of LPMs

We next assessed whether Bhlhe40 regulated induction of the alternative activation markers RELMα and Clec10a in LPMs in response to IL-4c. LPMs from *Bhlhe40*$^{+/+}$, *Bhlhe40*$^{-/-}$, *LysM-Cre*$^{-}$ *Bhlhe40*$^{fl/fl}$ and *LysM-Cre*$^{+}$ *Bhlhe40*$^{fl/fl}$ mice all induced these proteins following i.p. injection with IL-4c (Fig. 5a,b). In contrast, IL-4c increased the proportions of BrdU^{+} LPMs and pHH3^{+} LPMs by approximately 2-fold in *Bhlhe40*$^{+/+}$ and *LysM-Cre*$^{-}$ *Bhlhe40*$^{fl/fl}$ mice compared to *Bhlhe40*$^{-/-}$ and *LysM-Cre*$^{+}$ *Bhlhe40*$^{fl/fl}$ mice (Fig. 5c,d). IL-4c treatment also elicited a greater increase in the fraction of LPMs in the G1, S and G2M phases of the cell cycle in *Bhlhe40*$^{+/+}$ compared to *Bhlhe40*$^{-/-}$ mice (Fig. 5e). Immunoblot analysis of cyclins D1–D3, cyclin dependent kinase (CDK) 2, CDK4, CDK6 and the transcription factor E2F2, which regulate the G1 and S phases of the cell cycle[44], showed increases in cyclin D3, CDK2 and CDK4 in LPMs from IL-4c-treated compared to naïve mice (Supplementary Fig. 3); however, their abundance was generally similar in *Bhlhe40*$^{+/+}$ and *Bhlhe40*$^{-/-}$ LPMs (Supplementary Fig. 3). In contrast to cyclins and CDKs, E2F2 was similar in LPMs from mice injected or not with IL-4c (Supplementary Fig. 3). 7-AAD^{+} necrotic LPMs were somewhat increased in IL-4c-injected *Bhlhe40*$^{-/-}$ and *LysM-Cre*$^{+}$ *Bhlhe40*$^{fl/fl}$ mice compared to *Bhlhe40*$^{+/+}$ and *LysM-Cre*$^{-}$ *Bhlhe40*$^{fl/fl}$ mice (Fig. 5f). In mixed bone marrow chimeras (generated and reconstituted as in Fig. 2a–f) injected i.p. with IL-4c, a lower proportion of *Bhlhe40*$^{-/-}$ LPMs incorporated BrdU compared to *Bhlhe40*$^{+/+}$ LPMs within the same recipient (Supplementary Fig. 3).

We used transmission electron microscopy of bulk peritoneal cells from naïve and IL-4c-treated *Bhlhe40*$^{+/+}$ and *Bhlhe40*$^{-/-}$ mice to assess cell morphology. *Bhlhe40*$^{+/+}$ and *Bhlhe40*$^{-/-}$ LPMs from IL-4c-treated mice showed increases in cell size and endoplasmic reticulum (ER) extent compared to naïve LPMs (Supplementary Fig. 4). We observed no distinct morphology between naïve *Bhlhe40*$^{-/-}$ and *Bhlhe40*$^{+/+}$ LPMs, while LPMs from IL-4c-treated *Bhlhe40*$^{-/-}$ mice were somewhat larger and more vacuolated than LPMs from IL-4c-treated *Bhlhe40*$^{+/+}$ mice, without any severe morphologic defects (Supplementary Fig. 4). Therefore, Bhlhe40 was required for LPMs to rapidly cycle in response to IL-4c, but was dispensable for normal morphology and induction of alternative activation markers.

Monocytes can acquire a Bhlhe40-dependent proliferative program

Next we asked whether Bhlhe40 was required for the IL-4c-induced proliferation of other macrophages. IL-4c injection i.p. into *Bhlhe40*$^{GFP+}$ mice did not change the expression of GFP in LPMs, SPMs, AMs, kidney macrophages, red pulp macrophages and Kupffer cells compared to these populations in PBS-treated *Bhlhe40*$^{GFP+}$ mice (Supplementary Fig. 5). IL-4c injection i.p. into *Bhlhe40*$^{+/+}$ and *Bhlhe40*$^{-/-}$ mice resulted in equivalent BrdU incorporation by, and numbers of, red pulp macrophages, Kupffer cells and AMs (Fig. 5g and Supplementary Fig. 5), in contrast to LPMs and large pleural macrophages, which

required Bhlhe40 for a normal population of BrdU-incorporating cells in response to IL-4c (Fig. 5g and Supplementary Fig. 5).

Injection of thioglycollate and IL-4c i.p. causes monocyte-derived macrophages to proliferate and acquire alternative activation markers[17,18]. When we asked whether Bhlhe40 was expressed in these monocyte-derived macrophages, we found that the combination of thioglycollate and IL-4c induced marked expression of GFP in the thioglycollate-elicited macrophages in *Bhlhe40*$^{GFP+}$ mice compared to a lower expression of GFP in macrophages elicited by thioglycollate alone (Fig. 5h). After treatment with thioglycollate and IL-4c, *Bhlhe40*$^{-/-}$ mice had severely reduced proportions of BrdU^{+} and pHH3^{+} thioglycollate-elicited macrophages compared to *Bhlhe40*$^{+/+}$ mice (Fig. 5i,j and Supplementary Fig. 6), while RELMα was acquired normally (Supplementary Fig. 6). Thus, these data indicate that Bhlhe40 is a specific regulator of large serous cavity macrophage proliferation in response to IL-4c and that monocyte-derived macrophages can acquire a Bhlhe40-dependent proliferative program similar to that of serous cavity resident macrophages.

Bhlhe40 regulates LPM proliferation in response to *H. polygyrus*

The intestinal helminth *Heligmosomoides polygyrus bakeri* (*H. polygyrus*) is a natural mouse pathogen that elicits robust proliferation of LPMs following oral infection[14]. Infection with *H. polygyrus* caused a 4-fold increase in the number of LPMs in infected *Bhlhe40*$^{+/+}$ mice compared to *Bhlhe40*$^{-/-}$ mice after 8 days (Fig. 6a,b). Similar findings were obtained in *LysM-Cre*$^{-}$ *Bhlhe40*$^{fl/fl}$ and *LysM-Cre*$^{+}$ *Bhlhe40*$^{fl/fl}$ mice (Fig. 6b). Furthermore, after *H. polygyrus* infection, the proportions of BrdU^{+} LPMs and pHH3^{+} LPMs were reduced in *Bhlhe40*$^{-/-}$ and *LysM-Cre*$^{+}$ *Bhlhe40*$^{fl/fl}$ compared to *Bhlhe40*$^{+/+}$ and *LysM-Cre*$^{-}$ *Bhlhe40*$^{fl/fl}$ mice (Fig. 6c,d). *H. polygyrus* infection elicited a greater increase in the fraction of LPMs in the G1, S and G2M phases of the cell cycle in *Bhlhe40*$^{+/+}$ compared to *Bhlhe40*$^{-/-}$ mice (Fig. 6e). The proportion of 7-AAD^{+} necrotic LPMs was also increased in *Bhlhe40*$^{-/-}$ and *LysM-Cre*$^{+}$ *Bhlhe40*$^{fl/fl}$ compared to *Bhlhe40*$^{+/+}$ and *LysM-Cre*$^{-}$ *Bhlhe40*$^{fl/fl}$ infected mice (Fig. 6f). These data suggested that Bhlhe40 is essential for the proliferation of LPMs during type 2 immunity.

Bhlhe40 controls cell cycle-related transcription

To determine the effects of Bhlhe40 on the expression profile of LPMs during type 2 immunity, we performed gene expression microarrays on sorted LPMs from IL-4c-treated *Bhlhe40*$^{+/+}$, *Bhlhe40*$^{-/-}$ and *LysM-Cre*$^{+}$ *Bhlhe40*$^{fl/fl}$ mice after 4 days. More genes (254; Fig. 7a–c) were differentially expressed by 2-fold or more between LPMs from IL-4c-treated *Bhlhe40*$^{+/+}$ and *Bhlhe40*$^{-/-}$ mice compared to LPMs from naive *Bhlhe40*$^{+/+}$ and *Bhlhe40*$^{-/-}$ mice (87 genes; Fig. 7a–c). To ask whether the transcriptional changes that occurred in alternatively activated LPMs were dependent on Bhlhe40, we selected the 55 genes most differentially expressed (≥10-fold different) between naive and IL-4c-treated *Bhlhe40*$^{+/+}$ LPMs, including *Mgl2*, *Chil3*, *Arg1* and *Il1rl1* (Fig. 7d). These genes were generally normally expressed in *Bhlhe40*$^{+/+}$, *Bhlhe40*$^{-/-}$ and *LysM-Cre*$^{+}$ *Bhlhe40*$^{fl/fl}$ LPMs from IL-4c-treated mice (Fig. 7d), and we also found no defect in the expression of *Myo18a*, *C1qa*, *C1qb* and *C1qc*, which encode known regulators of LPM proliferation during type 2 immune responses[15] (Supplementary Fig. 7). Consistent with impaired proliferation, *Maf*

(3.2-fold) and *Mafb* (3.8-fold) were more highly expressed in *Bhlhe40*$^{-/-}$ compared to *Bhlhe40*$^{+/+}$ LPMs by qRT-PCR (Fig. 7e). Gene set enrichment analysis (GSEA) for Hallmark gene sets[45] showed prominent enrichment of gene sets related to proliferation, including the E2F targets and Myc targets v1 gene sets in the gene expression data between LPMs from IL-4c-treated *Bhlhe40*$^{+/+}$ and *Bhlhe40*$^{-/-}$ mice (Fig. 7f). Further comparison of differentially expressed genes to the C5 gene ontology sets indicated that LPMs from IL-4c-treated *Bhlhe40*$^{+/+}$ mice were substantially enriched for cell cycle and chromosome-related gene sets (Cell cycle, Cell cycle process, Mitotic cell cycle), while LPMs from IL-4c-treated *Bhlhe40*$^{-/-}$ mice showed enrichment for the Vacuole gene set (Fig. 7g–i), consistent with increased vacuolar area by electron microscopy. Therefore, Bhlhe40 was required in LPMs for normal regulation of cell cycle-related gene expression.

Bhlhe40 targets cell cycle-related loci directly

We next addressed whether Bhlhe40 regulated LPM gene expression via direct binding to gene loci by sorting LPMs from naïve and IL-4c-treated *Bhlhe40*$^{+/+}$ mice after 4 days for Bhlhe40 chromatin immunoprecipitation sequencing (ChIP-seq). Motif analysis of the called peaks identified the expected CACGTG E-box sequence (Fig. 8a) and a majority of Bhlhe40 peaks (naïve 2,245 total peaks; IL-4c-treated 5,011 total peaks) were promoter-associated in both samples (Fig. 8b). In both conditions, Bhlhe40 bound sites in the *Bhlhe40* (single peak, within promoter) and *Il10* (single peak, 1 kilobase (kb) downstream of locus) loci previously described in T cells (Fig. 8c and Supplementary Fig. 7)[33]. We also identified a novel Bhlhe40 binding site 1.5kb downstream of the *Bhlhe40* locus that was occupied only in LPMs from IL-4c-treated mice **(**Fig. 8c**)**. Many Bhlhe40 peaks were shared between LPMs from naïve and IL-4c-treated mice (1,684 sites, including peaks proximal to the *Klf4*, *Nr1d1*, *Plac8* and *Yy1* loci) (Fig. 8d), but the majority were unique to LPMs from IL-4c-treated mice (3,364 sites, including peaks proximal to the *Klf4* and *Nr1d1* loci) (Fig. 8d), often in association with shared peaks (as for the *Bhlhe40* locus).

Because Bhlhe40 and PU.1 may cooperate in LPMs[35], we compared our ChIP-seq data with previously published PU.1 ChIP-seq performed on LPMs from naïve C57BL/6 mice[35]. PU.1 peaks overlapped with 22% or 24% of Bhlhe40 peaks in LPMs from naïve or IL-4c-treated mice, respectively, including the *Clec10a*, *Ccl2* and *Plac8* loci (Fig. 8e,f and Supplementary Fig. 7). However, the majority of Bhlhe40 peaks (naïve 1,754 peaks; IL-4c 3,822 peaks) were not associated with PU.1 binding (Fig. 8f), including at the *Bhlhe40*, *Maf* and *Il10* loci. When we assessed whether Bhlhe40 bound directly to genes with Bhlhe40-dependent expression, we found that Bhlhe40 bound a small fraction of genes differentially expressed by two-fold or more between LPMs from naïve *Bhlhe40*$^{+/+}$ and *Bhlhe40*$^{-/-}$ mice **(**11% of genes downregulated in *Bhlhe40*$^{-/-}$ LPMs, 17% of genes upregulated in *Bhlhe40*$^{-/-}$ LPMs, Fig. 8g and Supplementary Fig. 7) and bound a greater fraction of genes differentially expressed between LPMs from IL-4c-treated *Bhlhe40*$^{+/+}$ and *Bhlhe40*$^{-/-}$ mice **(**15% of genes downregulated in *Bhlhe40*$^{-/-}$ LPMs, 48% of genes upregulated in *Bhlhe40*$^{-/-}$ LPMs, Fig. 8g and Supplementary Fig. 7), suggesting a direct role for Bhlhe40 in regulating gene expression in LPMs.

Further analysis of our ChIP-Seq data identified a Bhlhe40 peak within the *Maf* promoter in LPMs from naïve or IL-4c-treated mice (Fig. 8h), as well as two additional peaks closest to the *Maf* locus (200kb downstream (naïve and IL-4c) and 300kb downstream (IL-4c) of the locus) (Supplementary Fig. 7), suggesting that Bhlhe40 repressed the *Maf* locus. There was no clear Bhlhe40 peak uniquely associated with the *Mafb* locus (Supplementary Fig. 7). To address whether Bhlhe40 directly regulated other cell cycle-related loci, we performed GSEA analysis for the subset of genes directly bound by Bhlhe40 using the gene expression data from LPMs from IL-4c-treated *Bhlhe40*$^{+/+}$ and *Bhlhe40*$^{-/-}$ mice. We found that differential expression of these genes between *Bhlhe40*$^{+/+}$ and *Bhlhe40*$^{-/-}$ LPMs from IL-4c-treated mice largely recapitulated the enrichment of cell cycle-related modules observed when all gene expression data were analyzed (Fig. 8i and Supplementary Fig. 8). Thus, Bhlhe40 functioned in LPMs as a direct transcriptional regulator of numerous genomic loci, including those encoding cell cycle-related proteins.

Discussion

Here we found that the transcription factor Bhlhe40 was an essential cell-intrinsic regulator of proliferation in LPMs. In the steady-state, *Bhlhe40*$^{-/-}$ LPMs were reduced in number and a higher proportion accumulated in the G1 phase compared to *Bhlhe40*$^{+/+}$ LPMs. During type 2 immunity, Bhlhe40 was essential for normal proliferation and accumulation, with a reduced proportion of *Bhlhe40*$^{-/-}$ LPMs in the S and M phases compared to *Bhlhe40*$^{+/+}$ LPMs, but Bhlhe40 was dispensable for acquisition of alternative activation markers. Bhlhe40 mediated repression of *Maf* and activation of multiple proliferation-related loci to allow LPM cell cycling. Bhlhe40 was a tissue-specific regulator of proliferation of LPMs, but could be acquired by peritoneal monocyte-derived macrophages to support a proliferative program.

How deletion of Bhlhe40 impairs cell cycle progression of LPMs remains unclear. We observed that a higher proportion of *Bhlhe40*$^{-/-}$ LPMs were Ki67^{+} compared to *Bhlhe40*$^{+/+}$ LPMs, suggesting that *Bhlhe40*$^{-/-}$ LPMs might inappropriately enter the cell cycle. However, our data are not consistent with this notion, as we saw a selective increase in the proportion of *Bhlhe40*$^{-/-}$ LPMs in the G1 phase, without a commensurate increase in LPMs in the S, G2, or M phases. Both *Bhlhe40*$^{+/+}$ and *Bhlhe40*$^{-/-}$ LPMs upregulated cyclins and CDKs when mice were treated with IL-4c. In contrast, *Bhlhe40*$^{+/+}$ and *Bhlhe40*$^{-/-}$ LPMs had low expression of cyclins and CDKs at steady-state. These data support the notion that impaired progression from the G1 phase rather than enhanced proliferation was the primary cause of accumulation of G1 phase LPMs in naïve and likely IL-4c-treated *Bhlhe40*$^{-/-}$ mice. As expression of cyclin D and CDKs were comparable between *Bhlhe40*$^{+/+}$ and *Bhlhe40*$^{-/-}$ LPMs, alterations solely in the expression of these regulators likely do not explain the effect of Bhlhe40 deficiency on LPM proliferation. Instead, the phenotype of *Bhlhe40*$^{-/-}$ LPMs was probably due to the impaired transcriptional regulation of a broad set of cell cycle-related genes caused by loss of Bhlhe40 and upregulation of c-Maf and MafB.

Bhlhe40 and c-Maf may functionally interact in T cells[32,34]. Our data suggest that Bhlhe40 is a transcriptional repressor of *Maf* in LPMs. In contrast to T cells and other tissue-resident macrophages, LPMs require Bhlhe40 to support normal proliferation, suggesting that

Bhlhe40-mediated repression of *Maf* has distinct effects in different cell types. Expression of both Bhlhe40 and c-Maf in LPMs results in a unique regulatory interaction not detected in macrophage subsets lacking expression of one of these transcription factors. Downregulation of *Maf* and *Mafb* expression is critical for proliferation in macrophages[6,7]. Our data are most consistent with a role for Bhlhe40 in repressing *Maf* and *Mafb* to permit LPM cell cycling, along with Bhlhe40-mediated regulation of a wider set of target genes, some of them co-bound by PU.1, as previously proposed[35]. It is likely that specific networks of integrated transcriptional regulators control the development and function of resident macrophages in each tissue. In LPMs, this network would include Bhlhe40, PU.1[35], c-Maf[7] and MafB[7], as well as GATA6[9,10,11] and C/EBPβ[46], two transcription factors whose loss results in impaired development of LPMs.

In addition to LPMs and large pleural macrophages, AMs and, in some contexts, monocyte-derived macrophages expressed Bhlhe40. *Bhlhe40*$^{-/-}$ AMs only showed minor transcriptional differences compared to *Bhlhe40*$^{+/+}$ AMs and no evidence of a proliferative defect. c-Maf and MafB were poorly expressed in AMs[7] and were not induced in *Bhlhe40*$^{-/-}$ AMs (data not shown), suggesting that Bhlhe40 was not required to repress these transcription factors in AMs. It is also possible that Bhlhe41, which is expressed highly in AMs but not LPMs (data not shown) and can partially substitute for Bhlhe40[28], may compensate for the absence of Bhlhe40 in AMs. In contrast to AMs, monocyte-derived macrophages can acquire a Bhlhe40-dependent proliferative program in response to thioglycollate and IL-4c. The similarities of this Bhlhe40-regulated transcriptional program in monocyte-derived macrophages to that of LPMs remain to be explored.

Whether common regulators can control macrophage cell cycling in response to different stimuli during homeostasis (e.g. CSF-1) or type 2 immunity (e.g. IL-4, IL-5, or IL-13)[13] is unclear. Our findings demonstrate the existence of shared regulation of macrophage proliferation in the steady-state and disease, as well as a crucial role for tissue-specific transcriptional regulation acting in concert with more broadly shared regulators like c-Maf. This suggests the possibility of therapeutically targeting the proliferation of select macrophage populations, including tumor-associated macrophages (TAMs), which are known to partly derive from tissue-resident macrophages and locally proliferate[47,48,49,50].

Our results illustrate the complexity of tissue-specific control of macrophages, demonstrating that tissue-specific transcription factors are critical for the regulation of macrophage proliferation in health and disease. Our data provide direct evidence that resident macrophages are under constant control by a partnership of shared and tissue-specific transcription factors, with possible implications for therapies.

Methods

Mice

C57BL/6 (Taconic), B6.SJL (CD45.1, Taconic or Jackson), *Il10*$^{-/-}$ (B6.129P2-Il10tm1Cgn/J, Jackson) and *LysM-Cre* (B6N.129P2(B6)-*Lyz2*$^{tm1(cre)Ifo}$/J, Jackson) mice were obtained from the vendors listed. *Bhlhe40*$^{-/-}$ (10 generations backcrossed to the C57BL/6 background)[31,51], *Bhlhe40*$^{GFP+}$(10 generations backcrossed to the C57BL/6

background[21]) and *Bhlhe40*$^{fl/fl}$([33]) mice have been previously reported. The *Bhlhe40*$^{GFP+}$ mouse strain, originally defined as STOCK Tg(Bhlhe40-EGFP)PX84Gsat/Mmucd, identification number 034730-UCD, was obtained from the Mutant Mouse Regional Resource Center (MMRRC), a NCRR-NIH funded strain repository, and was donated to the MMRRC by the NINDS funded GENSAT BAC transgenic project (The GENSAT Project, NINDS Contract #N01NS02331 to the Rockefeller University). All mice were maintained in our specific pathogen free animal facility. Sex-matched littermates were used for experiments whenever possible, although in some cases mice from multiple litters were used in a single experiment. All animal experiments were approved by the Animal Studies Committee of Washington University in St. Louis.

Bone marrow chimeras

Bhlhe40$^{+/+}$ CD45.1/CD45.2 mice were lethally irradiated with 1,000 rads from a gamma irradiator, followed by same-day i.v. transfer of 16 million total bone marrow cells (8 million *Bhlhe40*$^{+/+}$ (CD45.1) cells plus either 8 million *Bhlhe40*$^{+/+}$ (CD45.2) or *Bhlhe40*$^{-/-}$ (CD45.2) cells). Mice were given drinking water containing sulfamethoxazole (1.3 mg/ml) and trimethoprim (0.26 mg/ml) for 2 weeks after irradiation and were allowed to reconstitute for at least 8 weeks. In some experiments, chimeras were also made with CD45.1 recipients using CD45.1/CD45.2 and CD45.2 donor bone marrow cells.

Peritoneal cell transfers

Peritoneal cells were lavaged from the peritonea of *Bhlhe40*$^{+/+}$ (CD45.1), *Bhlhe40*$^{+/+}$ (CD45.2), and *Bhlhe40*$^{-/-}$ (CD45.2) donors, and aliquots of cells were analyzed by flow cytometry to determine the frequency of LPMs. Bulk peritoneal cells were then transferred i.p. into resting *Bhlhe40*$^{+/+}$ recipients (CD45.1/CD45.2) at ratios resulting in the transfer of equal numbers of LPMs from each donor (200,000–300,000 LPMs).

Treatment of mice with thioglycollate and interleukin-4 complexes (IL-4c)

A 3% solution of thioglycollate was prepared in water, autoclaved and aged for three or more months[43]. Mice received 1 ml i.p. to induce peritonitis or a control injection of PBS[43]. IL-4c were prepared fresh as described[12,52]. IL-4 (Shenandoah Biotechnology #200–18, resuspended in 0.1% BSA in water) and anti-IL-4 antibody (clone 11B11; Leinco I-1071 or BioXCell BE0045) were combined in a 1:5 ratio by mass and a 1:1 ratio by volume, using ~1 mg/ml cytokine and ~5 mg/ml antibody. Complexes were incubated for ~2 minutes at room temperature (RT), diluted in 1x Dulbecco's PBS (DPBS) and injected i.p. Control injections were 0.1% BSA diluted in 1x DPBS, while naïve mice were also used for assessment of cell cycling, due to acquisition of Ki67^{+} by LPMs 2 days after PBS injection as described[13]. Mice received injections on day 0 and day 2, followed by sacrifice on day 4 as described[12]. For treatment with thioglycollate and IL-4c complexes, mice were injected i.p. with thioglycollate on day 0 and IL-4c on days 0 and 2, as previously described[17,18].

H. polygyrus infections

H. polygyrus bakeri third-stage larvae (L3) were prepared as described[53]. Mice were orally gavaged with 200 L3 or water (mock) with a 20-gauge ball-tipped gavage needle. Mice were sacrificed on day 8 of infection for assessment of peritoneal cells.

Leukocyte collection from tissues

Peritoneal and pleural cells were collected from body cavities by lavage. Bone marrow was collected by flushing hind limb femurs and tibias. Blood was collected by submandibular bleeding into EDTA or lithium heparin tubes. Lungs, liver, spleen and kidney were excised, placed in Iscove's Modified Dulbecco's Medium (IMDM) containing 5% fetal bovine serum (FBS), minced finely, and digested at 37 °C for an hour with mechanical disruption with a stir bar and enzymatic digestion (lung and kidneys, 4 mg/ml collagenase D (Roche); spleen, 0.25 g/ml collagenase B (Roche) and 30U/ml DNase I (EMD); liver, 4 mg/ml collagenase D and 30U/ml DNase I). Microglia[21] and small intestinal lamina propria cells[54] were isolated as described. After digestion, enzymes were inactivated with 5 mM EDTA and samples were incubated on ice for 5 minutes.

All cells were passed through a 70 μm cell strainer before analysis. If necessary, tissues were treated with ACK lysis buffer to lyse red blood cells. Cells were counted with a hemocytometer using 3% acetic acid (naïve peritoneum and pleura) or trypan blue (all others).

Flow cytometry

Cell surface staining was conducted in sterile 1x PBS with 0.5% BSA and 2 mM EDTA (hereafter FACS buffer). In brief, cells were washed in FACS buffer, blocked with α-CD16/32 (clone 2.4G2, BioXCell) for 10 minutes at 4 °C, stained for 20 min at 4 °C and washed with FACS buffer before flow cytometry. In some experiments to assess cell death, 7-AAD (1:20 of a 50 μg/mL solution, BioLegend or BD) was added to cells for 15 minutes prior to flow cytometry. Flow cytometry was performed on FACSCanto II, LSRFortessa, LSRFortessa X20 and LSR II instruments (all BD). FlowJo software (Treestar) was used for analysis. Antibodies and fluorescent dyes used in this study are listed in Supplementary Table 1.

Gating of cell populations was as follows (all analysis pre-gated on FSC/SSC and a FSC-W/FSC-A singlet gate). Blood monocytes were gated as $Ly6G^{-}CD115^{+}$ and then divided by Ly6C expression. Peritoneal and pleural macrophages were gated as $CD115^{+}CD11b^{+}$, then divided into $ICAM2^{+}MHC\text{-}II^{int}$ large macrophages and $ICAM2^{-}MHC\text{-}II^{+}$ small macrophages. Thioglycollate-elicited macrophages were gated as $CD115^{+}CD11b^{+}ICAM2^{lo}$. Liver Kupffer cells were gated as $CD45^{+}CD11b^{lo}F4/80^{hi}$, and in some contexts as $Ly6C^{-}$. Kidney macrophages were gated as $CD45^{+}Ly6C^{-}CD11b^{+}F4/80^{hi}$. AMs were gated as $CD45^{+}Siglec\text{-}F^{+}CD11c^{+}$, and in some contexts as $F4/80^{+}CD11b^{-}$. Red pulp macrophages were gated as $F4/80^{hi}$ and negative or low for other markers ($CD11b^{lo}$, $MHC\text{-}II^{lo}$, or $CD11c^{lo}$). Microglia were gated as $CD45^{int}CD11b^{+}$. Small intestinal lamina propria macrophages were gated as $CD45^{+}Ly6C^{-}F4/80^{+}CD64^{+}MHC\text{-}II^{+}$. Peritoneal B cells were

gated as CD115^{-}MHC-II^{+}CD19^{+}. Analysis of cells from the *Bhlhe40*$^{GFP+}$ reporter mouse used viability dyes (Po pro 1 or 7-AAD) when necessary to exclude dead cells.

Intracellular staining for flow cytometry

For Ki67, DAPI, RELMα, BrdU and pHH3 staining, the eBioscience FoxP3/Transcription Factor Staining Buffer set (00-5523-00) or the BioLegend True-Nuclear Transcription Factor Buffer set (424401) was used. In brief, after surface staining, cells were fixed with 1x Fix Concentrate buffer in provided Fix Diluent for 30 minutes at 4 °C. Cells were then washed with FACS buffer and stored overnight. To permeabilize the cells, samples were washed with 1x Perm buffer diluted in water. Following blocking with 2% rat serum, samples were stained for 1 hour at RT, except for DAPI and secondary antibodies (20 minutes at RT), followed by washing in 1x Perm buffer and FACS buffer before flow cytometry.

For BrdU staining, mice were given 1 mg of BrdU i.p. (from BD kit, 552598, or Sigma, B5002) three hours before sacrifice as described[12]. After sacrifice of mice and peritoneal lavage, samples were processed, fixed and stored overnight as for other intracellular antigens. BrdU-labelled cells were washed in 1x Perm buffer, incubated in DNase I (from BD kit, 552598 or Sigma, D4513) in 1x DPBS for 30 min at 37 °C, washed in 1x Perm buffer, blocked with 2% rat serum and stained for 1 hour at RT with α-BrdU antibody (BD, 552598), followed by washing in 1x Perm buffer and FACS buffer. Mice that did not receive BrdU were used as negative controls.

Transmission electron microscopy

For ultrastructural analyses, peritoneal cells were fixed in 2% PFA/2.5% glutaraldehyde (Polysciences Inc.) in 100 mM sodium cacodylate buffer, pH 7.2 for 1 hour at RT. Samples were washed in sodium cacodylate buffer at RT and postfixed in 1% osmium tetroxide (Polysciences Inc.) for 1 hour. Samples were rinsed in distilled water prior to en bloc staining with 1% aqueous uranyl acetate (Ted Pella Inc.) for 1 hour. Following rinsing in distilled water, samples were dehydrated in a graded series of ethanol and embedded in Eponate 12 resin (Ted Pella Inc.). Sections of 95 nm were cut with a Leica Ultracut UCT ultramicrotome, stained with uranyl acetate and lead citrate and viewed on a JEOL 1200 EX transmission electron microscope (JEOL USA Inc.) equipped with an AMT 8 megapixel digital camera and AMT Image Capture Engine V602 software (Advanced Microscopy Techniques).

For morphological analysis, images were blinded and randomized. LPMs were identified as large cells with abundant cytoplasm and were distinguished from rare peritoneal mast cells by the absence of electron-dense granules. For measurement statistics, the ObjectJ plugin was used in ImageJ software (NIH). In brief, cell and vesicle cross-sectional area were calculated by tracing the outline of the cell or vesicles, respectively, and calculating the enclosed area. ER cross-sectional extent was calculated by tracing the ER with lines and adding these lengths together. For assessment of ER luminal width, a randomly placed grid was used to subdivide the cell into sections. Representative measurements were then taken across the lumen of the ER, and the measurements from each section were averaged.

Microarrays

The following cell populations were sorted on a FACSAria II (BD) into FBS: for naïve LPM microarrays, $B220^{-}F4/80^{+}CD11b^{+}ICAM2^{+}$ LPMs from untreated mice; for *in vivo* IL-4c-stimulated LPM microarrays, $CD115^{+}CD11b^{+}ICAM2^{+}MHC\text{-}II^{int}$ LPMs from mice treated with IL-4c at days 0 and 2, with peritoneal cells collected at day 4; for naïve AM microarrays, $CD45^{+}Ly6G^{-}Siglec\text{-}F^{+}CD11c^{+}CD11b^{lo}$ AMs from untreated mice. Cells were lysed and RNA was purified using the E.Z.N.A. MicroElute Total RNA kit (Omega Bio-Tek). Total RNA was submitted to the Genome Technology Access core at Washington University for cDNA synthesis (NuGen Pico SL) followed by microarray analysis on the Affymetrix Mouse Gene 1.0 ST platform. Data were analyzed using the DNASTAR ArrayStar program. Genes with an expression value of <5 (in log 2 scale) in all replicates were considered not expressed. For analysis of naïve microarrays, which were conducted on three biologic replicates, the differentially expressed gene list was also filtered on genes with a p-value significance of ≤0.05 by the moderated *t*-test. For analysis of *in vivo* IL-4c-stimulated LPM microarrays, which were conducted on two biologic replicates, no p-value filtering was applied. For comparison of naïve to *in vivo* IL-4c-stimulated LPMs, CEL files were normalized together to generate expression data. Heatmaps were generated with Morpheus (software.broadinstitute.org/morpheus/). Venn diagrams were generated with the Venn Diagram Plotter tool (Pacific Northwest National Laboratories, omics.pnl.gov). Multiple differentially expressed probe sets representing a single gene were presented in heat maps without exclusion, but only unique genes were counted in Venn diagrams.

The macrophage alternative activation gene signature used to assess naïve macrophages was generated from GSE69607 comparing M0, M1 and M2 bone marrow-derived macrophages (BMDMs)[55]. The 29 genes 20-fold upregulated in M2 vs. M1 BMDMs were used to define a set of macrophage alternative activation-related genes. The LPM gene signature was previously published[36]. For the LPM alternative activation gene signature used to assess *in vivo* IL-4c-stimulated LPMs, we compared our microarray data from naïve and *in vivo* IL-4c-stimulated $Bhlhe40^{+/+}$ LPMs and defined an alternative activation signature for LPMs, composed of the 55 unique genes up- or down-regulated by ten-fold or more. For comparison of the gene expression signature of Bhlhe40- or GATA6-deficient LPMs, our data was analyzed in parallel with GSE37448[11] as above, as both data sets were generated on the Affymetrix Mouse Gene 1.0 ST platform.

Quantitative real-time polymerase chain reaction (qRT-PCR)

LPMs were sorted as for microarrays. RNA was isolated with the E.Z.N.A. MicroElute Total RNA kit (Omega Bio-Tek), and cDNA was synthesized with 50 ng RNA using the High Capacity RNA to cDNA kit (Invitrogen). RNA concentration was assessed with a Nanodrop 2000 spectrophotometer (ThermoFisher). qRT-PCR was performed with Power SYBR Green PCR Master Mix (Applied Biosystems) using a StepOnePlus Real-Time PCR machine (Applied Biosystems). Gene expression was determined relative to Hprt by the ΔC_T method. The following primers were used: *Hprt*, forward 5′-TCAGTCAACGGGGGACAT AAA-3′, reverse 5′-GGGGCTGTACTGCTTAACCAG-3′; *Maf* forward 5’-GGAGACCGACCGCATCATC-3’ reverse 5’-TCATCCAGTAGTAGTCTTCCAGG-3’;

Mafb forward 5’-TTCGACCTTCTCAAGTTCGACG-3’, reverse 5’-TCGAGATGGGTCTTCGGTTCA-3’.

Immunoblotting

LPMs were sorted as for microarrays, pooled from multiple mice and lysed at a concentration of 25 million cells/mL using the RIPA lysis buffer system (Santa Cruz Biotechnology). Laemmli buffer (Bio-Rad, with added 2-mercaptoethanol) was added to the samples, which were then boiled for 10 minutes, and run on a Bio-Rad Miniprotean TGX gel with Precision Plus Dual Color molecular weight standards (Bio-Rad). Proteins were transferred to a BioBlot polyvinylidine fluoride membrane (Costar). Blots were blocked for 1–2 hours with 5% milk, followed by overnight staining with primary antibodies in 5% milk at 4 °C with shaking. After washing, blots were stained with horseradish peroxidase-conjugated secondary antibodies for 45–60 minutes at RT with shaking. After washing, blots were developed with either Super Signal West Femto Maximum Sensitivity Substrate (Thermo Fisher) or Clarity Western ECL Substrate (Bio-Rad). Images were captured on a Chemidoc system (Bio-Rad) and inverted on Adobe Illustrator for presentation. Blots were stripped with Restore PLUS Western Blot Stripping Buffer (ThermoFisher). Blots were then washed, reblocked and restained. Antibodies used are listed in Supplementary Table 1.

Gene set enrichment analysis

Lists of differentially expressed genes (≥1.5-fold up- or downregulated) were cross-referenced to the C5 gene sets in the MSigDB database. To further examine the enrichment of gene sets, the GSEA software from the Broad Institute was used to analyze all expressed genes or all Bhlhe40-bound expressed genes for gene set enrichment using the Hallmark and C5 databases[42,45].

ChIP-seq

Anti-Bhlhe40 ChIP-seq was performed as previously published[33]. LPMs were sorted as for microarrays and pooled from multiple mice. Cells were fixed for 10 min at RT in 1% PFA with shaking. Cross-linking was stopped with glycine added to 0.125 M, cells were pelleted and dry pellets were stored at −80 °C. Cross-linked chromatin was sonicated and immunoprecipitated using rabbit anti-Dec1 (Bhlhe40) antibody (NB100–1800, Lot C1; Novus Biologicals). Following immunoprecipitation, the GenElute PCR cleanup kit (Sigma) was used to purify DNA. Library construction was followed by single-read sequencing on a HiSeq3000 (Illumina) at the Genome Technology Access Center at Washington University in St. Louis. Read length was 50 base pairs (bp). Quality control of FASTQ files used FastQC (0.11.3). Bowtie (1.1.1) was used to map reads onto the mm10 mouse reference genome. Input DNA samples were used for peak calling on Bhlhe40-immunoprecipitation samples using MACS v1.4 with default settings[56]. Generated peaks were additionally required to have fold-enrichment ≥5 and reads from unmapped regions (chrUn_xxxxx) were excluded.

Normalized tracks were generated with Deeptools (2.5.3), and tracks were visualized with the UCSC Genome Browser. Discriminative Regular Expression Motif Elicitation (DREME) (5.0.1)[57] was used for motif enrichment analysis using 250 bp flanked summits of all

acquired peaks. To annotate peaks, R package ChIPseeker (1.14.1) was used. The intersect function from the BEDtools suite (v2.25.0) was used to find shared peaks. The shared peak count was defined as the number of overlapping peaks in the naïve LPM Bhlhe40 ChIP-seq sample compared to the *in vivo* IL-4c-stimulated LPM Bhlhe40 ChIP-seq sample. Two group Venn diagrams were generated with the Venn Diagram Plotter tool.

ChIP-seq data for PU.1 performed on LPMs (GSM1533894) and the corresponding input sample (GSM1533895)[35] were downloaded in SRA format and converted to FASTQ format using the fastq-dump function (v2.8.1) from the SRA Toolkit. Subsequent processing and filtration was performed as described above. The shared peak count was defined as the number of overlapping peaks in the naïve LPM Bhlhe40 ChIP-seq sample compared to each of the other samples, except for the comparison of *in vivo* IL-4c-stimulated LPM Bhlhe40 ChIP-seq and LPM PU.1 ChIP-seq samples, which was defined as the number of overlapping peaks in the IL-4c Bhlhe40 sample. Three group Venn diagrams were generated with the eulerAP3 v3 tool (www.eulerdiagrams.org/eulerAPE/)[58].

Statistical analysis

All data are from at least two independent experiments, unless otherwise indicated. Data were analyzed by paired or unpaired two-tailed Student's *t*-tests (Prism 7; GraphPad Software, Inc.) as indicated in the figure legends, with $p \leq 0.05$ considered significant. For relevant comparisons where no p-value is shown, the p-value was > 0.05. For analysis of gene lists against the MSigDB database, the hypergeometric test performed by the Investigate Gene Sets tool was used to determine significance. For GSEA analysis, the NES score calculated by the GSEA software was used to account for set size effects when determining enrichment. The GSEA-calculated FWER p-value was used to determine significance, as this statistic is more conservative than the False Discovery Rate (FDR). Horizontal bars represent the mean and error bars represent the standard error of the mean (s.e.m.).

Reporting summary

Further information on experimental design is available in the Nature Research Reporting Summary linked to this article.

Data availability

The data that support the findings of this study are available from the corresponding author upon request. The microarray and ChIP-sequencing data have been deposited in the GEO repository under accession code GSE125730.

Supplementary Material

Refer to Web version on PubMed Central for supplementary material.

Acknowledgements

This work was supported by the National Institute of Allergy and Infectious Disease (NIAID) (AI113118 and AI132653) (B.T.E.) and a Burroughs Wellcome Fund Career Award for Medical Scientists (B.T.E.). N.N.J. was

supported by grant 5T32AI007163 from the NIAID. C.-C.L. was supported by the McDonnell International Scholars Academy at Washington University. S.C.-C.H. was supported by the Case Comprehensive Cancer Center American Cancer Society IRG Award (IRG-16-186-21). M.E.C. was supported by the National Science Foundation Graduate Research Fellowship program (DGE-1745038). Research reported in this publication was supported by the Washington University Institute of Clinical and Translational Sciences grant UL1TR002345 from the National Center for Advancing Translational Sciences (NCATS) of the National Institutes of Health (NIH). The content is solely the responsibility of the authors and does not necessarily represent the official view of the NIH. We thank E. Lantelme, A. Cullen and D. Brinja for help with fluorescence activated cell-sorting. We thank W. Beatty and L. Mwaghore for electron microscopy. We thank S. Van Dyken and C. Farnsworth for critical reading of the manuscript. We thank the members of the G. Randolph laboratory for helpful discussions about this project. We thank J. Bando, M. Robinette and T. Ai for help with flow cytometry of the gut.

References

1. Ginhoux F et al. Fate mapping analysis reveals that adult microglia derive from primitive macrophages. Science 330, 841–845 (2010). [PubMed: 20966214]
2. Schulz C et al. A lineage of myeloid cells independent of Myb and hematopoietic stem cells. Science 336, 86–90 (2012). [PubMed: 22442384]
3. T'Jonck W, Guilliams M & Bonnardel J Niche signals and transcription factors involved in tissue-resident macrophage development. Cell. Immunol 330, 43–53 (2018). [PubMed: 29463401]
4. Hashimoto D et al. Tissue-resident macrophages self-maintain locally throughout adult life with minimal contribution from circulating monocytes. Immunity 38, 792–804 (2013). [PubMed: 23601688]
5. Yona S et al. Fate mapping reveals origins and dynamics of monocytes and tissue macrophages under homeostasis. Immunity 38, 79–91 (2013). [PubMed: 23273845]
6. Aziz A, Soucie E, Sarrazin S & Sieweke MH MafB/c-Maf deficiency enables self-renewal of differentiated functional macrophages. Science 326, 867–871 (2009). [PubMed: 19892988]
7. Soucie EL et al. Lineage-specific enhancers activate self-renewal genes in macrophages and embryonic stem cells. Science 351, 680–693 (2016).
8. Imperatore F et al. SIRT1 regulates macrophage self-renewal. EMBO J. 36, 2353–2372 (2017). [PubMed: 28701484]
9. Rosas M et al. The transcription factor Gata6 links tissue macrophage phenotype and proliferative renewal. Science 344, 645–648 (2014). [PubMed: 24762537]
10. Okabe Y & Medzhitov R Tissue-specific signals control reversible program of localization and functional polarization of macrophages. Cell 157, 832–844 (2014). [PubMed: 24792964]
11. Gautier EL et al. Gata6 regulates aspartoacylase expression in resident peritoneal macrophages and controls their survival. J. Exp. Med 211, 1525–1531 (2014). [PubMed: 25024137]
12. Jenkins SJ et al. Local macrophage proliferation, rather than recruitment from the blood, is a signature of TH2 inflammation. Science 332, 1284–1288 (2011). [PubMed: 21566158]
13. Jenkins SJ et al. IL-4 directly signals tissue-resident macrophages to proliferate beyond homeostatic levels controlled by CSF-1. J. Exp. Med 210, 2477–2491 (2013). [PubMed: 24101381]
14. Ruckerl D & Allen JE Macrophage proliferation, provenance, and plasticity in macroparasite infection. Immunol. Rev 262, 113–133 (2014). [PubMed: 25319331]
15. Minutti CM et al. Local amplifiers of IL-4Ralpha-mediated macrophage activation promote repair in lung and liver. Science 356, 1076–1080 (2017). [PubMed: 28495878]
16. Bosurgi L et al. Macrophage function in tissue repair and remodeling requires IL-4 or IL-13 with apoptotic cells. Science 356, 1072–1076 (2017). [PubMed: 28495875]
17. Gundra UM et al. Alternatively activated macrophages derived from monocytes and tissue macrophages are phenotypically and functionally distinct. Blood 123, e110–122 (2014). [PubMed: 24695852]
18. Gundra UM et al. Vitamin A mediates conversion of monocyte-derived macrophages into tissue-resident macrophages during alternative activation. Nat. Immunol 18, 642–653 (2017). [PubMed: 28436955]

19. Kato Y, Kawamoto T, Fujimoto K & Noshiro M DEC1/STRA13/SHARP2 and DEC2/SHARP1 coordinate physiological processes, including circadian rhythms in response to environmental stimuli. Curr. Top. Dev. Biol 110, 339–372 (2014). [PubMed: 25248482]
20. Ow JR, Tan YH, Jin Y, Bahirvani AG & Taneja R Stra13 and sharp-1, the non-grouchy regulators of development and disease. Curr. Top. Dev. Biol 110, 317–338 (2014). [PubMed: 25248481]
21. Lin CC et al. IL-1-induced Bhlhe40 identifies pathogenic T helper cells in a model of autoimmune neuroinflammation. J. Exp. Med 213, 251–271 (2016). [PubMed: 26834156]
22. Sun H & Taneja R Stra13 expression is associated with growth arrest and represses transcription through histone deacetylase (HDAC)-dependent and HDAC-independent mechanisms. Proc. Natl. Acad. Sci. USA 97, 4058–4063 (2000). [PubMed: 10737769]
23. St-Pierre B, Flock G, Zacksenhaus E & Egan SE Stra13 homodimers repress transcription through class B E-box elements. J. Biol. Chem 277, 46544–46551 (2002). [PubMed: 12297495]
24. Li Y et al. The expression of antiapoptotic protein survivin is transcriptionally upregulated by DEC1 primarily through multiple sp1 binding sites in the proximal promoter. Oncogene 25, 3296–3306 (2006). [PubMed: 16462771]
25. Qian Y, Zhang J, Jung YS & Chen X DEC1 coordinates with HDAC8 to differentially regulate TAp73 and DeltaNp73 expression. PLoS One 9, e84015 (2014). [PubMed: 24404147]
26. Seimiya M et al. Impaired lymphocyte development and function in Clast5/Stra13/DEC1-transgenic mice. Eur. J. Immunol 34, 1322–1332 (2004). [PubMed: 15114665]
27. Kanda M et al. Transcriptional regulator Bhlhe40 works as a cofactor of T-bet in the regulation of IFN-γ production in iNKT cells. Proc. Natl. Acad. Sci. USA 113, E3394–3402 (2016). [PubMed: 27226296]
28. Kreslavsky T et al. Essential role for the transcription factor Bhlhe41 in regulating the development, self-renewal and BCR repertoire of B-1a cells. Nat. Immunol 18, 442–455 (2017). [PubMed: 28250425]
29. Camponeschi A et al. DEC1/STRA13 is a key negative regulator of activation-induced proliferation of human B cells highly expressed in anergic cells. Immunol. Lett 198, 7–11 (2018). [PubMed: 29601939]
30. Martinez-Llordella M et al. CD28-inducible transcription factor DEC1 is required for efficient autoreactive CD4+ T cell response. J. Exp. Med 210, 1603–1619 (2013). [PubMed: 23878307]
31. Lin CC et al. Bhlhe40 controls cytokine production by T cells and is essential for pathogenicity in autoimmune neuroinflammation. Nat. Commun 5, 3551 (2014). [PubMed: 24699451]
32. Yu F et al. The transcription factor Bhlhe40 is a switch of inflammatory versus antiinflammatory Th1 cell fate determination. J. Exp. Med 215, 1813–1821 (2018). [PubMed: 29773643]
33. Huynh JP et al. Bhlhe40 is an essential repressor of IL-10 during Mycobacterium tuberculosis infection. J. Exp. Med 215, 1823–1838 (2018). [PubMed: 29773644]
34. Gabryšová L & O'Garra A Regulating the regulator: Bhlhe40 directly keeps IL-10 in check. J. Exp. Med 215, 1767–1769 (2018). [PubMed: 29880485]
35. Gosselin D et al. Environment drives selection and function of enhancers controlling tissue-specific macrophage identities. Cell 159, 1327–1340 (2014). [PubMed: 25480297]
36. Gautier EL et al. Gene-expression profiles and transcriptional regulatory pathways that underlie the identity and diversity of mouse tissue macrophages. Nat. Immunol 13, 1118–1128 (2012). [PubMed: 23023392]
37. Lavin Y et al. Tissue-resident macrophage enhancer landscapes are shaped by the local microenvironment. Cell 159, 1312–1326 (2014). [PubMed: 25480296]
38. Scott CL et al. Bone marrow-derived monocytes give rise to self-renewing and fully differentiated Kupffer cells. Nat. Commun 7, 10321 (2016). [PubMed: 26813785]
39. Bain CC et al. Long-lived self-renewing bone marrow-derived macrophages displace embryo-derived cells to inhabit adult serous cavities. Nat. Commun 7, 11852 (2016).
40. Shaw TN et al. Tissue-resident macrophages in the intestine are long lived and defined by Tim-4 and CD4 expression. J. Exp. Med 215, 1507–1518 (2018). [PubMed: 29789388]

41. Kim KW et al. MHC II+ resident peritoneal and pleural macrophages rely on IRF4 for development from circulating monocytes. J. Exp. Med 213, 1951–1959 (2016). [PubMed: 27551152]
42. Subramanian A et al. Gene set enrichment analysis: a knowledge-based approach for interpreting genome-wide expression profiles. Proc. Natl. Acad. Sci. USA 102, 15545–15550 (2005). [PubMed: 16199517]
43. Gautier EL, Ivanov S, Lesnik P & Randolph GJ Local apoptosis mediates clearance of macrophages from resolving inflammation in mice. Blood 122, 2714–2722 (2013). [PubMed: 23974197]
44. Bertoli C, Skotheim JM, & de Bruin RA Control of cell cycle transcription during G1 and S phases. Nat. Rev. Mol. Cell. Biol 14, 518–528 (2013). [PubMed: 23877564]
45. Liberzon A et al. The Molecular Signatures Database (MSigDB) hallmark gene set collection. Cell. Syst 1, 417–425 (2015). [PubMed: 26771021]
46. Cain DW et al. Identification of a tissue-specific, C/EBPβ-dependent pathway of differentiation for murine peritoneal macrophages. J. Immunol 191, 4665–4675 (2013). [PubMed: 24078688]
47. Franklin RA & Li MO Ontogeny of tumor-associated macrophages and its implication in cancer regulation. Trends Cancer 2, 20–34 (2016). [PubMed: 26949745]
48. Zhu Y et al. Tissue-resident macrophages in pancreatic ductal adenocarcinoma originate from embryonic hematopoiesis and promote tumor progression. Immunity 47, 323–338 (2017). [PubMed: 28813661]
49. Loyher PL et al. Macrophages of distinct origins contribute to tumor development in the lung. J. Exp. Med 215, 2536–2553 (2018). [PubMed: 30201786]
50. Mantovani A, Marchesi F, Malesci A, Laghi L & Allavena P Tumour-associated macrophages as treatment targets in oncology. Nat. Rev. Clin. Oncol 14, 399–416 (2017). [PubMed: 28117416]

Online Methods References

51. Sun H, Lu B, Li RQ, Flavell RA & Taneja R Defective T cell activation and autoimmune disorder in Stra13-deficient mice. Nat. Immunol 2, 1040–1047 (2001). [PubMed: 11668339]
52. Finkelman FD et al. Anti-cytokine antibodies as carrier proteins. Prolongation of in vivo effects of exogenous cytokines by injection of cytokine-anti-cytokine antibody complexes. J. Immunol 151, 1235–1244 (1993). [PubMed: 8393043]
53. Camberis M, Le Gros G & Urban J Jr. Animal model of Nippostrongylus brasiliensis and Heligmosomoides polygyrus. Curr. Protoc. Immunol Chapter 19, Unit 19.12 (2003).
54. Bando JK et al. The tumor necrosis factor superfamily member RANKL suppresses effector cytokine production in group 3 innate lymphoid cells. Immunity 48, 1208–1219 (2018). [PubMed: 29858011]
55. Jablonski KA et al. Novel markers to delineate murine M1 and M2 Macrophages. PLoS One 10, e0145342 (2015). [PubMed: 26699615]
56. Zhang Y et al. Model-based analysis of ChIP-Seq (MACS). Genome Biol. 9, R137 (2008). [PubMed: 18798982]
57. Bailey TL DREME: motif discovery in transcription factor ChIP-seq data. Bioinformatics 27, 1653–1659 (2011). [PubMed: 21543442]
58. Micallef L & Rodgers P EulerAPE: drawing area-proportional 3-Venn diagrams using ellipses. PLoS One 9, e101717 (2014). [PubMed: 25032825]

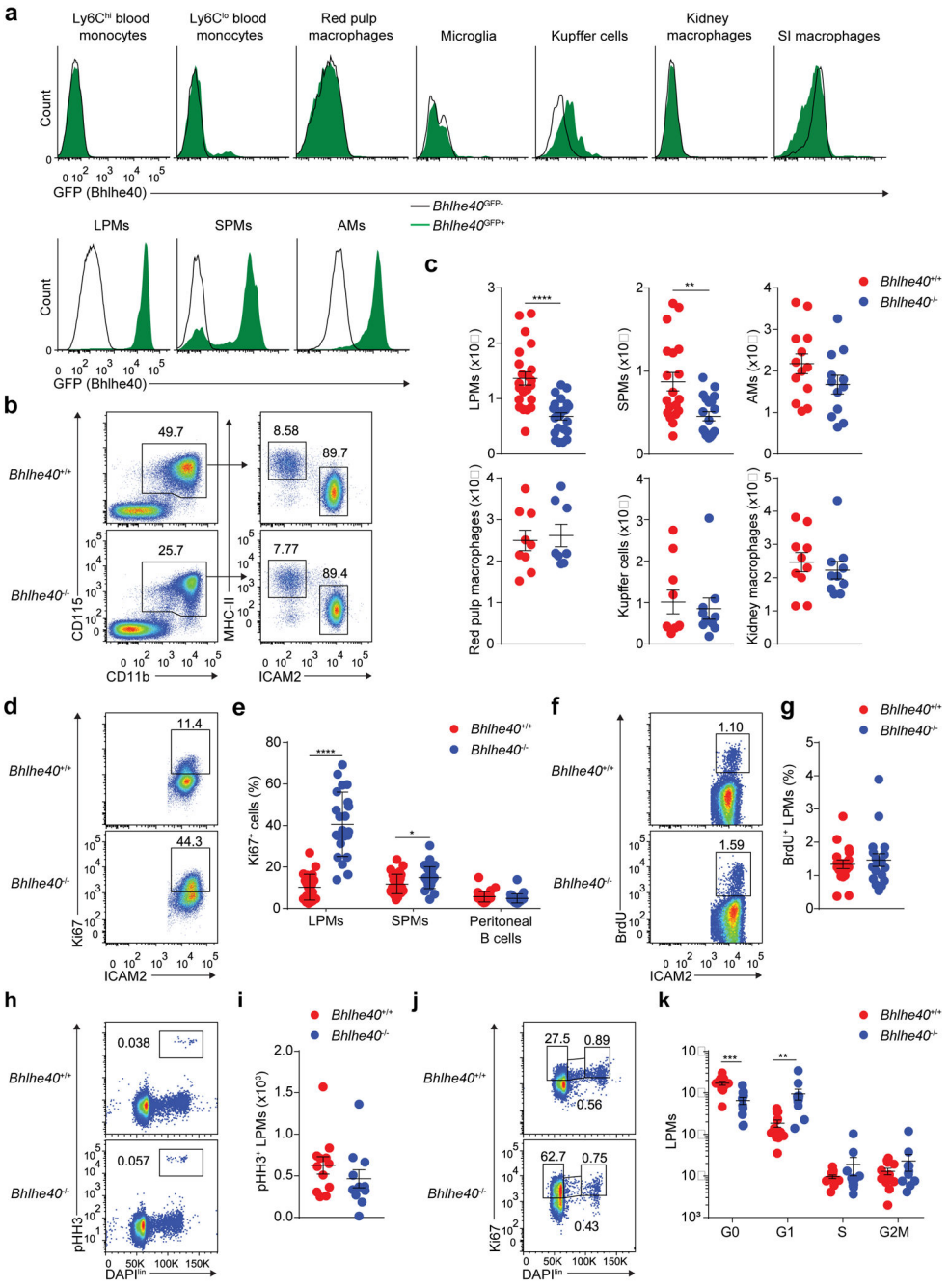

Figure 1. Loss of Bhlhe40 dysregulates the cell cycle in LPMs.

a, Flow cytometry of *Bhlhe40*^{GFP} transgene reporter expression in blood monocytes (representative of 2 experiments, n=5 *Bhlhe40*$^{GFP+}$, 2 *Bhlhe40*$^{GFP-}$); red pulp macrophages, microglia, Kupffer cells, kidney macrophages, SI macrophages, and peritoneal macrophages (representative of 2 experiments, n=4 *Bhlhe40*$^{GFP+}$, 2 *Bhlhe40*$^{GFP-}$); and AMs (representative of 3 experiments, n=6 *Bhlhe40*$^{GFP+}$, 3 *Bhlhe40*$^{GFP-}$) from *Bhlhe40*$^{GFP+}$ and *Bhlhe40*$^{GFP-}$ mice. **b**, Flow cytometry of peritoneal macrophage subsets in *Bhlhe40*$^{+/+}$ and *Bhlhe40*$^{-/-}$ mice (representative of 6 experiments, n=22/group). **c**, Numbers of LPMs as in **b**, SPMs (pooled from 5 experiments, n=19/group), AMs (pooled from 4 experiments, n=13

Bhlhe40$^{+/+}$, 12 *Bhlhe40*$^{-/-}$), red pulp macrophages (pooled from 3 experiments, n=9 *Bhlhe40*$^{+/+}$, 8 *Bhlhe40*$^{-/-}$), Kupffer cells, and kidney macrophages (both pooled from 2 experiments, n=10/group) from *Bhlhe40*$^{+/+}$ and *Bhlhe40*$^{-/-}$ mice. **d**, Flow cytometry of Ki67 expression by *Bhlhe40*$^{+/+}$ and *Bhlhe40*$^{-/-}$ LPMs (representative of 7 experiments, n=24 *Bhlhe40*$^{+/+}$, 22 *Bhlhe40*$^{-/-}$). **e**, Frequency of Ki67^{+} LPMs as in **d**, SPMs, and B cells (both pooled from 8 experiments, n=30 *Bhlhe40*$^{+/+}$, 29 *Bhlhe40*$^{-/-}$) from *Bhlhe40*$^{+/+}$ and *Bhlhe40*$^{-/-}$ mice. **f**, Flow cytometry of BrdU incorporation by *Bhlhe40*$^{+/+}$ and *Bhlhe40*$^{-/-}$ LPMs (representative of 5 experiments, n=18/group). **g**, Frequency of BrdU^{+} LPMs as in **f**. **h**, Flow cytometry of pHH3 expression by *Bhlhe40*$^{+/+}$ and *Bhlhe40*$^{-/-}$ LPMs (representative of 4 experiments, n=12 *Bhlhe40*$^{+/+}$, 11 *Bhlhe40*$^{-/-}$). **i**, Frequency of pHH3^{+} LPMs as in **h**. **j**, Flow cytometry for discrimination of cell cycle phases of *Bhlhe40*$^{+/+}$ and *Bhlhe40*$^{-/-}$ LPMs (representative of 4 experiments, n=12 *Bhlhe40*$^{+/+}$, 11 *Bhlhe40*$^{-/-}$). **k**, Numbers of LPMs in each phase of the cell cycle as in **j**. Data in **c,e,g,i,k** are mean ± s.e.m; each symbol represents an individual mouse (**c,e,g,i,k**). *$P \leq 0.05$; **$P < 0.01$; ***$P < 0.001$; ****$P < 0.0001$, unpaired two-sided Student's *t*-test.

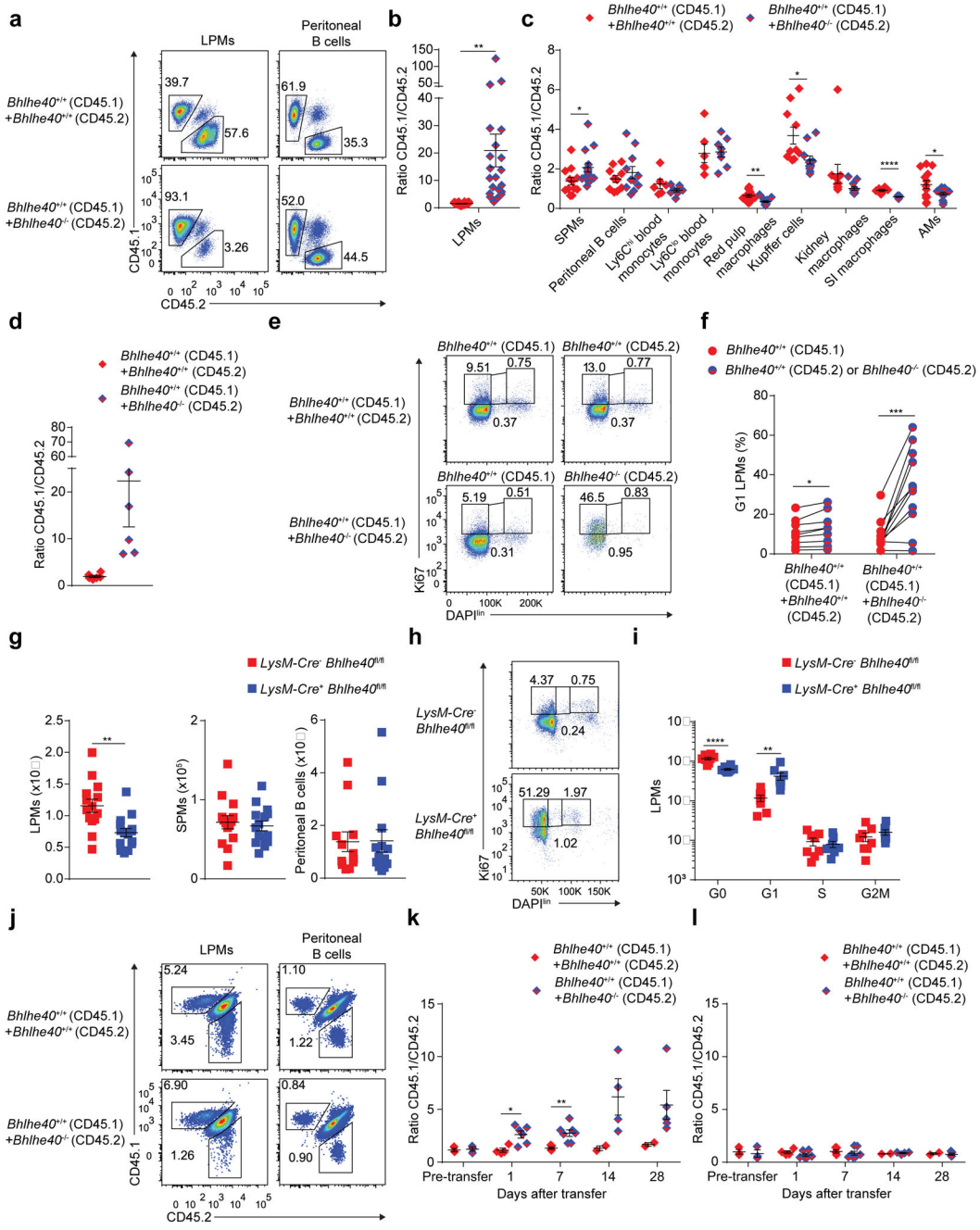

Figure 2. Bhlhe40 is cell-intrinsically required in LPMs to regulate the cell cycle.

a, Flow cytometry for the discrimination of donor and recipient LPMs (representative of 6 experiments, n=18 [*Bhlhe40*$^{+/+}$ (CD45.1) +*Bhlhe40*$^{+/+}$ (CD45.2)], 21 [*Bhlhe40*$^{+/+}$ (CD45.1) +*Bhlhe40*$^{-/-}$ (CD45.2)]) and peritoneal B cells (representative of 4 experiments, n=12 [*Bhlhe40*$^{+/+}$ (CD45.1) +*Bhlhe40*$^{+/+}$ (CD45.2)], 13 [*Bhlhe40*$^{+/+}$ (CD45.1) +*Bhlhe40*$^{-/-}$ (CD45.2)]) from *Bhlhe40*$^{+/+}$ (CD45.1) plus either *Bhlhe40*$^{+/+}$ (CD45.2) or *Bhlhe40*$^{-/-}$ (CD45.2) mixed bone marrow chimeras. **b**, Ratio of CD45.1 to CD45.2 LPMs as in **a**. **c**, Ratios of CD45.1 cells to CD45.2 cells for SPMs (pooled from 4 experiments, n=12 [*Bhlhe40*$^{+/+}$ (CD45.1) +*Bhlhe40*$^{+/+}$ (CD45.2)], 13 [*Bhlhe40*$^{+/+}$ (CD45.1) +*Bhlhe40*$^{-/-}$

(CD45.2)]), peritoneal B cells as in **a**, blood monocytes (pooled from 2 experiments, n=6 [*Bhlhe40*$^{+/+}$ (CD45.1) +*Bhlhe40*$^{+/+}$ (CD45.2)], 8 [*Bhlhe40*$^{+/+}$ (CD45.1) +*Bhlhe40*$^{-/-}$ (CD45.2)]), red pulp macrophages, AMs (both pooled from 6 experiments, n=13 [*Bhlhe40*$^{+/+}$ (CD45.1) +*Bhlhe40*$^{+/+}$ (CD45.2)], 15 [*Bhlhe40*$^{+/+}$ (CD45.1) +*Bhlhe40*$^{-/-}$ (CD45.2)]), Kupffer cells, kidney macrophages (both pooled from 3 experiments, n=10 [*Bhlhe40*$^{+/+}$ (CD45.1) +*Bhlhe40*$^{+/+}$ (CD45.2)], 11 [*Bhlhe40*$^{+/+}$ (CD45.1) +*Bhlhe40*$^{-/-}$ (CD45.2)]), and SI macrophages (pooled from 2 experiments, n=6 [*Bhlhe40*$^{+/+}$ (CD45.1) +*Bhlhe40*$^{+/+}$ (CD45.2)], 7 [*Bhlhe40*$^{+/+}$ (CD45.1) +*Bhlhe40*$^{-/-}$ (CD45.2)]) from mixed bone marrow chimeras. **d**, Ratio of CD45.1 to CD45.2 large pleural macrophages (pooled from 2 experiments, n=6/group) from mixed bone marrow chimeras. **e**, Flow cytometry for discrimination of cell cycle phases of *Bhlhe40*$^{+/+}$ (CD45.1), *Bhlhe40*$^{+/+}$ (CD45.2), or *Bhlhe40*$^{-/-}$ (CD45.2) LPMs from mixed bone marrow chimeras (representative of 3 experiments, n=9 [*Bhlhe40*$^{+/+}$ (CD45.1) +*Bhlhe40*$^{+/+}$ (CD45.2)], 11 [*Bhlhe40*$^{+/+}$ (CD45.1) +*Bhlhe40*$^{-/-}$ (CD45.2)]). **f**, Frequency of G1 LPMs as in **e**, with LPMs from each donor recovered from the same recipient connected by a line. **g**, Numbers of LPMs, SPMs (both pooled from 6 experiments, n=14 *LysM-Cre*$^{-}$ *Bhlhe40*$^{fl/fl}$, 15 *LysM-Cre*$^{+}$ *Bhlhe40*$^{fl/fl}$) and peritoneal B cells (5 experiments, n=12 *LysM-Cre*$^{-}$ *Bhlhe40*$^{fl/fl}$, 13 *LysM-Cre*$^{+}$ *Bhlhe40*$^{fl/fl}$) from *LysM-Cre*$^{-}$ *Bhlhe40*$^{fl/fl}$ and *LysM-Cre*$^{+}$ *Bhlhe40*$^{fl/fl}$ mice. **h**, Flow cytometry for discrimination of cell cycle phases of *LysM-Cre*$^{-}$ *Bhlhe40*$^{fl/fl}$ and *LysM-Cre*$^{+}$ *Bhlhe40*$^{fl/fl}$ LPMs (representative of 3 experiments, n=8/group). **i**, Numbers of LPMs in each phase of the cell cycle as in **h**. **j**, Flow cytometry for the discrimination of donor and recipient LPMs and peritoneal B cells from CD45.1/CD45.2 recipients of mixed peritoneal cells transferred from *Bhlhe40*$^{+/+}$ (CD45.1) plus either *Bhlhe40*$^{+/+}$ (CD45.2) or *Bhlhe40*$^{-/-}$ mice (CD45.2) mice (representative of 2 experiments, n=3 [*Bhlhe40*$^{+/+}$ (CD45.1) +*Bhlhe40*$^{+/+}$ (CD45.2)], 5 [*Bhlhe40*$^{+/+}$ (CD45.1) +*Bhlhe40*$^{-/-}$ (CD45.2)]). **k,l**, Ratio of CD45.1 LPMs to CD45.2 LPMs (**k**) and CD45.1 peritoneal B cells to CD45.2 peritoneal B cells (**l**) as in **j** (pooled from 2–3 experiments, n≥3 for all time points, except day 14 [*Bhlhe40*$^{+/+}$ (CD45.1) +*Bhlhe40*$^{+/+}$ (CD45.2)], n=2). Data in **b,c,d,f,g,i,k,l** are mean ± s.e.m; (**b,c,d,g,i,k,l**) each symbol or (**f**) paired symbols represent an individual mouse. *$P \leq 0.05$; **$P < 0.01$; ***$P < 0.001$; ****$P < 0.0001$, unpaired (**b,c,d,g,i,k,l**) or paired (**f**) two-sided Student's *t*-test.

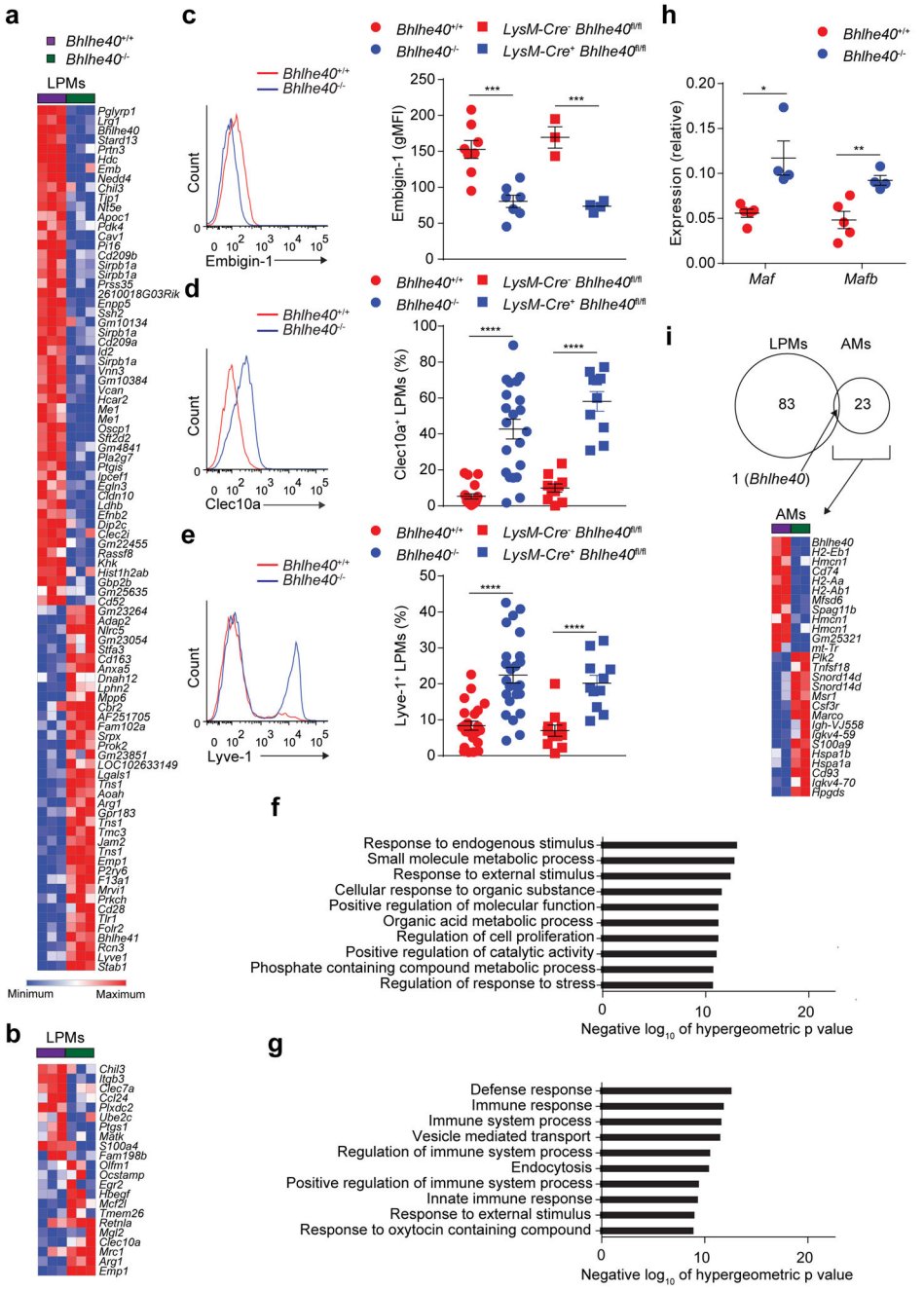

Figure 3. Bhlhe40 regulates a distinct set of genes related to alternative activation in LPMs.

a,b, Gene expression microarray data were analyzed for genes differentially expressed by ≥2-fold (**a**) and expression of a macrophage alternative activation gene signature in *Bhlhe40*$^{+/+}$ and *Bhlhe40*$^{-/-}$ LPMs (**b**). **c**, Flow cytometry of Embigin-1 expression and quantitation of geometric mean fluorescence intensity (gMFI) on LPMs (pooled from 4 experiments, n=8 *Bhlhe40*$^{+/+}$, 7 *Bhlhe40*$^{-/-}$; 1 experiment, n=3 *LysM-Cre*$^{-}$ *Bhlhe40*$^{fl/fl}$, 4 *LysM-Cre*$^{+}$ *Bhlhe40*$^{fl/fl}$). **d**, Flow cytometry of Clec10a expression and frequency of Clec10a^{+} LPMs (pooled from 6 experiments, n=19 *Bhlhe40*$^{+/+}$ and 21 *Bhlhe40*$^{-/-}$; 4 experiments, n=10 *LysM-Cre*$^{-}$ *Bhlhe40*$^{fl/fl}$ and *LysM-Cre*$^{+}$ *Bhlhe40*$^{fl/fl}$). **e** Flow cytometry

of Lyve-1 expression and frequency of Lyve-1$^+$ LPMs (pooled from 7 experiments, n=22 *Bhlhe40*$^{+/+}$, 24 *Bhlhe40*$^{-/-}$; 5 experiments, n=11 *LysM-Cre*$^-$ *Bhlhe40*$^{fl/fl}$ and *LysM-Cre*$^+$ *Bhlhe40*$^{fl/fl}$) from *Bhlhe40*$^{+/+}$, *Bhlhe40*$^{-/-}$, *LysM-Cre*$^-$ *Bhlhe40*$^{fl/fl}$, and *LysM-Cre*$^+$ *Bhlhe40*$^{fl/fl}$ LPMs. **f,g**, MSigDB C5 gene set enrichment was analyzed using the lists of genes expressed at ≥1.5-fold in *Bhlhe40*$^{+/+}$ vs. *Bhlhe40*$^{-/-}$ (**f**) or *Bhlhe40*$^{-/-}$ vs. *Bhlhe40*$^{+/+}$ LPMs (**g**). **h**, qRT-PCR of *Maf* and *Mafb* expression relative to *Hprt* in *Bhlhe40*$^{+/+}$ and *Bhlhe40*$^{-/-}$ LPMs (pooled from 2 experiments, n=5 *Bhlhe40*$^{+/+}$, 4 *Bhlhe40*$^{-/-}$). **i**, Gene expression microarray data were analyzed for shared and unique Bhlhe40-dependent genes in *Bhlhe40*$^{+/+}$ and *Bhlhe40*$^{-/-}$ LPMs and AMs (≥2-fold differentially expressed, depicted as a Venn diagram). Heat map depicts all genes differentially expressed by ≥2-fold in *Bhlhe40*$^{+/+}$ and *Bhlhe40*$^{-/-}$ AMs. Microarray data from LPMs (n=3/group) and AMs (n=2/group) are from a single experiment. Data in **c-e,h** are mean ± s.e.m; each symbol represents an individual mouse (**c-e,h**). *$P \leq 0.05$; **$P < 0.01$; ***$P < 0.001$; ****$P < 0.0001$, (**c-e,h**) unpaired two-sided Student's *t*-test and (**f,g**) one-sided hypergeometric test.

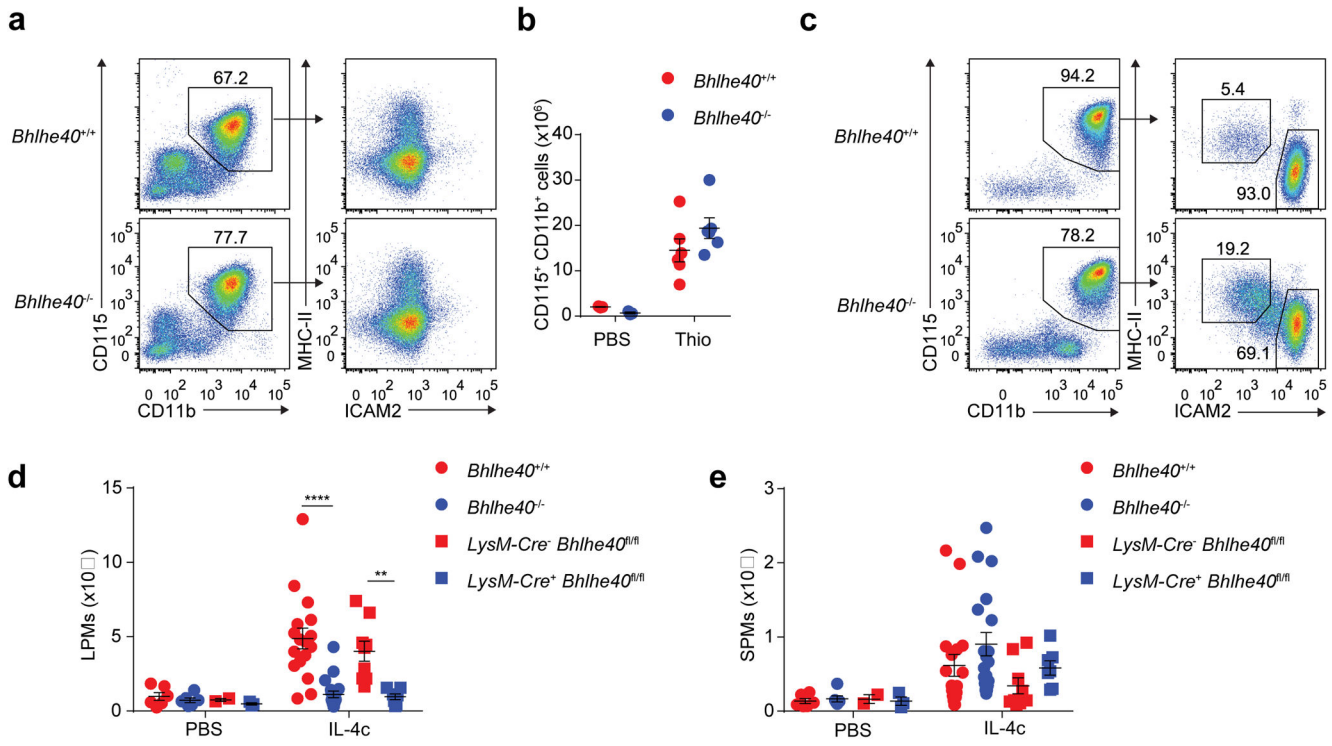

Figure 4. Bhlhe40 is required for normal accumulation of resident, but not recruited, macrophages in the peritoneum.

a, Flow cytometry of peritoneal macrophage subsets from *Bhlhe40*$^{+/+}$ and *Bhlhe40*$^{-/-}$ mice treated with thioglycollate (Thio) (representative of 3 experiments, n=6/group). **b**, Numbers of CD115^{+}CD11b^{+} peritoneal macrophages from *Bhlhe40*$^{+/+}$ and *Bhlhe40*$^{-/-}$ mice treated with PBS or Thio as in **a** (pooled from 3 experiments, n=3/group for PBS, 6/group for Thio). **c**, Flow cytometry of peritoneal macrophage subsets from *Bhlhe40*$^{+/+}$ and *Bhlhe40*$^{-/-}$ mice treated with IL-4c (representative of 6 experiments, 17 IL-4c-treated *Bhlhe40*$^{+/+}$, 19 IL-4c-treated *Bhlhe40*$^{-/-}$). **d,e**, Numbers of LPMs (**d**) and SPMs (**e**) as in **c** from *Bhlhe40*$^{+/+}$, *Bhlhe40*$^{-/-}$, *LysM-Cre*$^{-}$ *Bhlhe40*$^{fl/fl}$, and *LysM-Cre*$^{+}$ *Bhlhe40*$^{fl/fl}$ mice treated with PBS or IL-4c (pooled from 5 experiments, 6 PBS-treated *Bhlhe40*$^{+/+}$ and *Bhlhe40*$^{-/-}$; IL-4c-treated as in **c** for *Bhlhe40*$^{+/+}$ and *Bhlhe40*$^{-/-}$; 2 experiments, 2 PBS-treated *LysM-Cre*$^{-}$ *Bhlhe40*$^{fl/fl}$; 3 PBS-treated *LysM-Cre*$^{+}$ *Bhlhe40*$^{fl/fl}$; 9 IL-4c-treated *LysM-Cre*$^{-}$ *Bhlhe40*$^{fl/fl}$; 7 IL-4c-treated *LysM-Cre*$^{+}$ *Bhlhe40*$^{fl/fl}$). Data in **b,d,e** are mean ± s.e.m; each symbol represents an individual mouse (**b,d,e**). $^{**}P < 0.01$; $^{****}P < 0.0001$, unpaired two-sided Student's *t*-test.

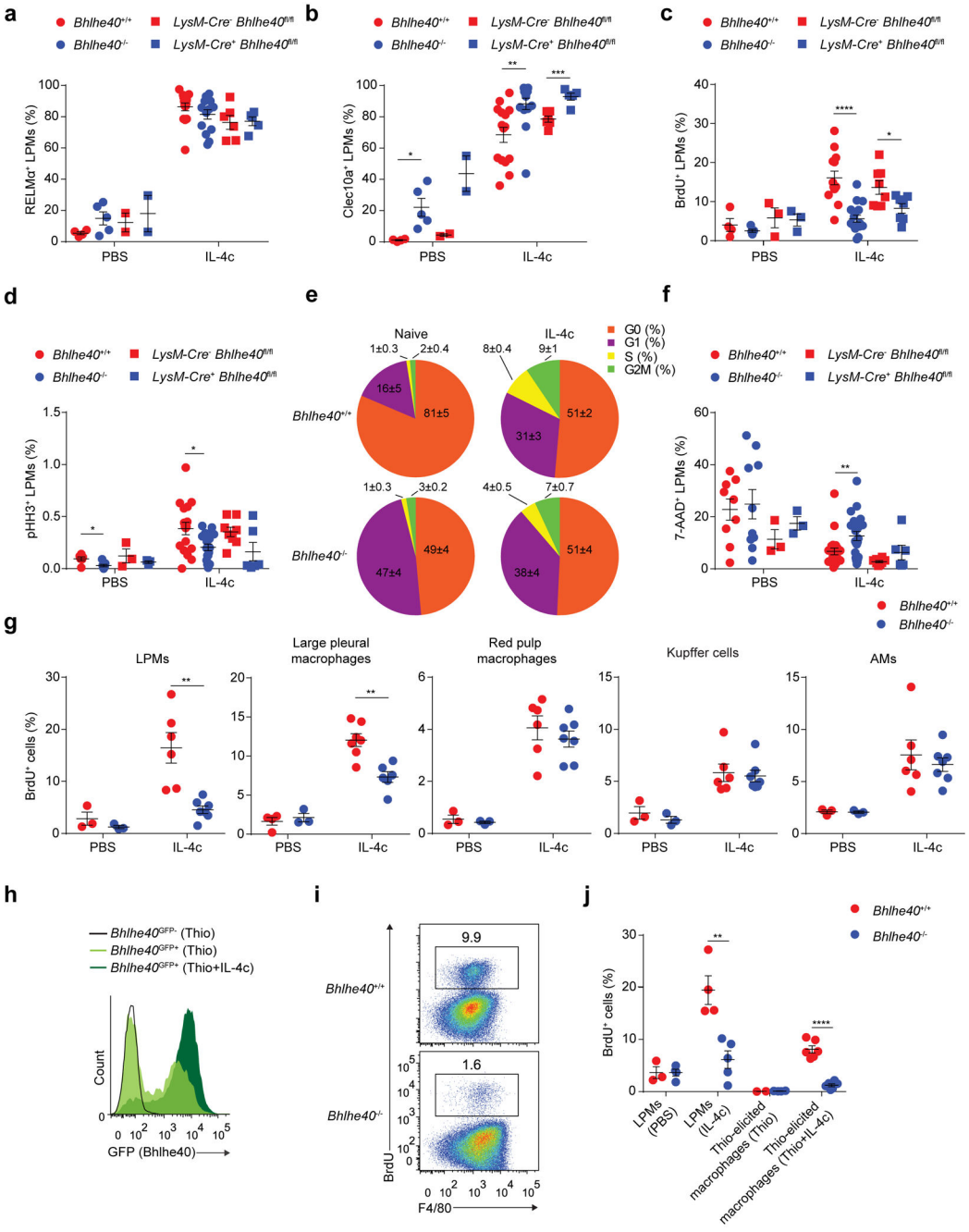

Figure 5. Bhlhe40 is required for normal cycling, but not polarization, of peritoneal macrophages during type 2 immunity.

a-d, Frequency of RELMα$^+$ LPMs (**a**) (pooled from 3 experiments, n=4 PBS-treated *Bhlhe40*$^{+/+}$ and *Bhlhe40*$^{-/-}$; 15 IL-4c-treated *Bhlhe40*$^{+/+}$ and *Bhlhe40*$^{-/-}$; 2 experiments, 2 PBS-treated *LysM-Cre*$^-$ *Bhlhe40*$^{fl/fl}$ and *LysM-Cre*$^+$ *Bhlhe40*$^{fl/fl}$; 6 IL-4c-treated *LysM-Cre*$^-$ *Bhlhe40*$^{fl/fl}$; 5 IL-4c-treated *LysM-Cre*$^+$ *Bhlhe40*$^{fl/fl}$), Clec10a$^+$ LPMs (**b**) (pooled as in **a**), BrdU$^+$ LPMs (**c**) (pooled from 3 experiments, n=4 PBS-treated *Bhlhe40*$^{+/+}$; 5 PBS-treated *Bhlhe40*$^{-/-}$; 13 IL-4c-treated *Bhlhe40*$^{+/+}$; 17 IL-4c-treated *Bhlhe40*$^{-/-}$; 3 PBS-treated *LysM-Cre*$^-$ *Bhlhe40*$^{fl/fl}$ and *LysM-Cre*$^+$ *Bhlhe40*$^{fl/fl}$; 8 IL-4c-treated *LysM-Cre*$^-$ *Bhlhe40*$^{fl/fl}$; 7

IL-4c-treated *LysM-Cre*$^{+}$ *Bhlhe40*$^{fl/fl}$), and pHH3^{+} LPMs (**d**) (pooled from 3 experiments, n=6 PBS-treated *Bhlhe40*$^{+/+}$; 7 PBS-treated *Bhlhe40*$^{-/-}$; 16 IL-4c-treated *Bhlhe40*$^{+/+}$; 18 IL-4c-treated *Bhlhe40*$^{-/-}$; 3 PBS-treated *LysM-Cre*$^{-}$ *Bhlhe40*$^{fl/fl}$ and *LysM-Cre*$^{+}$ *Bhlhe40*$^{fl/fl}$; 8 IL-4c-treated *LysM-Cre*$^{-}$ *Bhlhe40*$^{fl/fl}$; 6 IL-4c-treated *LysM-Cre*$^{+}$ *Bhlhe40*$^{fl/fl}$) from *Bhlhe40*$^{+/+}$, *Bhlhe40*$^{-/-}$, *LysM-Cre*$^{-}$ *Bhlhe40*$^{fl/fl}$, and *LysM-Cre*$^{+}$ *Bhlhe40*$^{fl/fl}$ mice treated with PBS or IL-4c. **e**, Proportion of LPMs in each phase of the cell cycle from *Bhlhe40*$^{+/+}$ and *Bhlhe40*$^{-/-}$ mice unstimulated or treated with IL-4c (pooled from 5 experiments, n=6/group for unstimulated; 16 IL-4c-treated *Bhlhe40*$^{+/+}$; 15 IL-4c-treated *Bhlhe40*$^{-/-}$). **f**, Frequency of 7-AAD^{+} LPMs from *Bhlhe40*$^{+/+}$, *Bhlhe40*$^{-/-}$, *LysM-Cre*$^{-}$ *Bhlhe40*$^{fl/fl}$, and *LysM-Cre*$^{+}$ *Bhlhe40*$^{fl/fl}$ mice treated with PBS or IL-4c (pooled from 3 experiments, n=5 PBS-treated *Bhlhe40*$^{+/+}$ and *Bhlhe40*$^{-/-}$; 13 IL-4c-treated *Bhlhe40*$^{+/+}$; 17 IL-4c-treated *Bhlhe40*$^{-/-}$; 3 PBS-treated *LysM-Cre*$^{-}$ *Bhlhe40*$^{fl/fl}$ and *LysM-Cre*$^{+}$ *Bhlhe40*$^{fl/fl}$; 8 IL-4c-treated *LysM-Cre*$^{-}$ *Bhlhe40*$^{fl/fl}$; 7 IL-4c-treated *LysM-Cre*$^{+}$ *Bhlhe40*$^{fl/fl}$). **g**, Frequency of BrdU^{+} LPMs, large pleural macrophages, red pulp macrophages, Kupffer cells, and AMs from *Bhlhe40*$^{+/+}$ and *Bhlhe40*$^{-/-}$ mice treated with PBS or IL-4c (pooled from 2 experiments, n=3/group for PBS; 6 IL-4c-treated *Bhlhe40*$^{+/+}$; 7 IL-4c-treated *Bhlhe40*$^{-/-}$; except for pleura, 3 experiments, n=4 PBS-treated *Bhlhe40*$^{+/+}$; 3 PBS-treated *Bhlhe40*$^{-/-}$; 7 IL-4c-treated *Bhlhe40*$^{+/+}$; 6 IL-4c-treated *Bhlhe40*$^{-/-}$). **h**, Flow cytometry of *Bhlhe40*^{GFP} transgene reporter expression in thioglycollate (Thio)-elicited macrophages from *Bhlhe40*$^{GFP+}$ and *Bhlhe40*$^{GFP-}$ mice treated with Thio or Thio and IL-4c (1 experiment, n=2 Thio-treated *Bhlhe40*$^{GFP+}$; 3 Thio and IL-4c-treated *Bhlhe40*$^{GFP+}$; 1 Thio-treated *Bhlhe40*$^{GFP-}$). **i**, Flow cytometry of BrdU incorporation by Thio-elicited macrophages from *Bhlhe40*$^{+/+}$ and *Bhlhe40*$^{-/-}$ mice treated with Thio and IL-4c (representative of 2 experiments, n=6/group). **j**, Frequency of BrdU^{+} LPMs and Thio-elicited macrophages from *Bhlhe40*$^{+/+}$ and *Bhlhe40*$^{-/-}$ mice treated with PBS, IL-4c, Thio, or Thio and IL-4c (pooled from 2 experiments, n=3 PBS-treated *Bhlhe40*$^{+/+}$, 4 PBS-treated *Bhlhe40*$^{-/-}$, 4 IL-4c-treated *Bhlhe40*$^{+/+}$, 5 IL-4c-treated *Bhlhe40*$^{-/-}$, 2 Thio-treated *Bhlhe40*$^{+/+}$, 4 Thio-treated *Bhlhe40*$^{-/-}$, Thio and IL-4c-treated as in **i**). Data in **a-f,g,j** are mean ± s.e.m; each symbol represents an individual mouse (**a-d,f,g,j**). *$P \leq 0.05$; **$P < 0.01$; ***$P < 0.001$; ****$P < 0.0001$, unpaired two-sided Student's *t*-test.

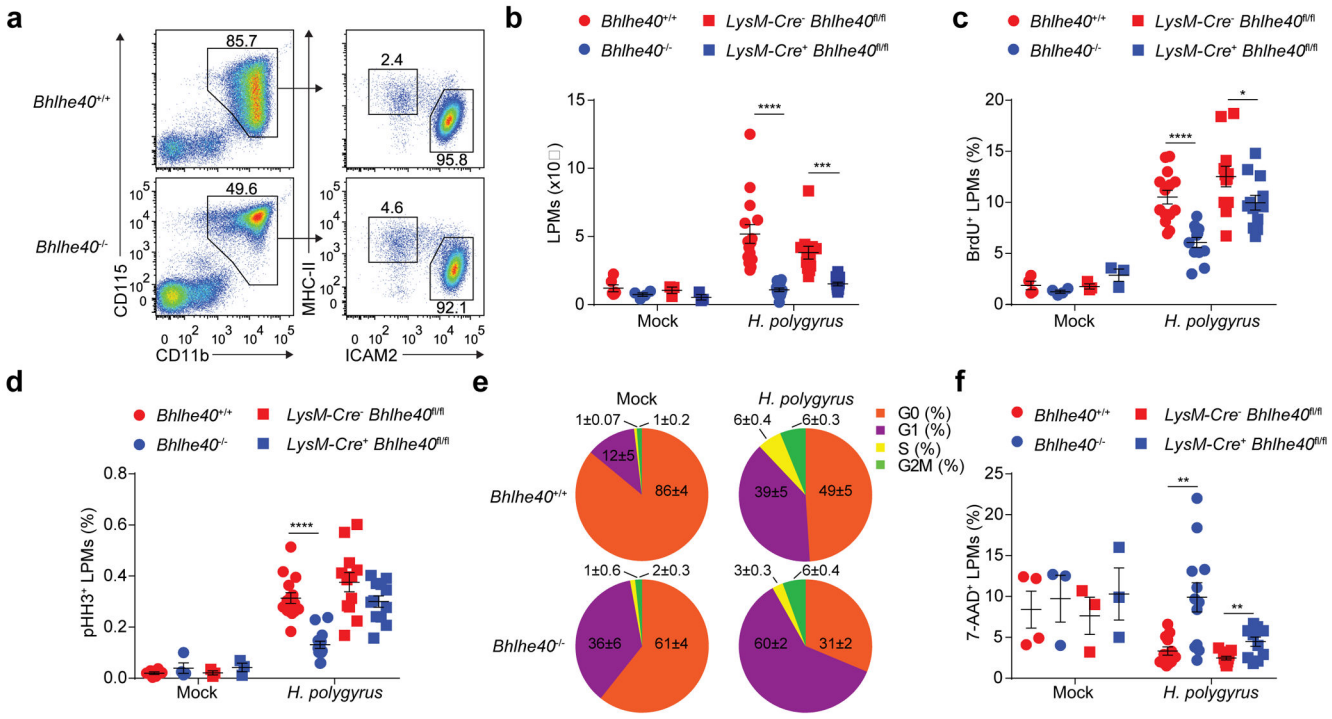

Figure 6. Bhlhe40 is required for LPM proliferation in response to *H. polygyrus*.

a, Flow cytometry of peritoneal macrophage subsets from *Bhlhe40*$^{+/+}$ and *Bhlhe40*$^{-/-}$ mice infected with *H. polygyrus* (representative of 4 experiments, n=15 *Bhlhe40*$^{+/+}$, 14 *Bhlhe40*$^{-/-}$). **b**, Numbers of LPMs from *Bhlhe40*$^{+/+}$, *Bhlhe40*$^{-/-}$, *LysM-Cre*$^{-}$ *Bhlhe40*$^{fl/fl}$, and *LysM-Cre*$^{+}$ *Bhlhe40*$^{fl/fl}$ mice mock- or *H.polygyrus*-infected as in **a** (pooled from 3 experiments, n=6 mock-infected *Bhlhe40*$^{+/+}$; 4 mock-infected *Bhlhe40*$^{-/-}$; *H. polygyrus*-infected as in **a** for *Bhlhe40*$^{+/+}$ and *Bhlhe40*$^{-/-}$; 3 mock-infected *LysM-Cre*$^{-}$ *Bhlhe40*$^{fl/fl}$ and *LysM-Cre*$^{+}$ *Bhlhe40*$^{fl/fl}$; 12 *H. polygyrus*-infected *LysM-Cre*$^{-}$ *Bhlhe40*$^{fl/fl}$ and *LysM-Cre*$^{+}$ *Bhlhe40*$^{fl/f}$). **c,d**, Frequency of BrdU^{+} LPMs (**c**) (pooled from 3 experiments, n=4 mock-infected *Bhlhe40*$^{+/+}$ and *Bhlhe40*$^{-/-}$; 14 *H. polygyrus*-infected *Bhlhe40*$^{+/+}$; 12 *H. polygyrus*-infected *Bhlhe40*$^{-/-}$; 3 mock-infected *LysM-Cre*$^{-}$ *Bhlhe40*$^{fl/fl}$ and *LysM-Cre*$^{+}$ *Bhlhe40*$^{fl/fl}$; 12 *H. polygyrus*-infected *LysM-Cre*$^{-}$ *Bhlhe40*$^{fl/fl}$ and *LysM-Cre*$^{+}$ *Bhlhe40*$^{fl/fl}$) and pHH3^{+} LPMs (**d**) (pooled from 3 experiments, n=6 mock-infected *Bhlhe40*$^{+/+}$; 4 mock-infected *Bhlhe40*$^{-/-}$; 15 *H. polygyrus*-infected *Bhlhe40*$^{+/+}$; 14 *H. polygyrus*-infected *Bhlhe40*$^{-/-}$; 3 mock-infected *LysM-Cre*$^{-}$ *Bhlhe40*$^{fl/fl}$ and *LysM-Cre*$^{+}$ *Bhlhe40*$^{fl/fl}$; 12 *H. polygyrus*-infected *LysM-Cre*$^{-}$ *Bhlhe40*$^{fl/fl}$ and *LysM-Cre*$^{+}$ *Bhlhe40*$^{fl/fl}$) from *Bhlhe40*$^{+/+}$, *Bhlhe40*$^{-/-}$, *LysM-Cre*$^{-}$ *Bhlhe40*$^{fl/fl}$, and *LysM-Cre*$^{+}$ *Bhlhe40*$^{fl/fl}$ mice mock- or *H. polygyrus*-infected. **e**, Proportion of LPMs in each phase of the cell cycle from *Bhlhe40*$^{+/+}$ and *Bhlhe40*$^{-/-}$ mice mock- or *H. polygyrus*-infected (pooled from 2 experiments, n=3 mock-infected *Bhlhe40*$^{+/+}$, 2 mock-infected *Bhlhe40*$^{-/-}$, 7 *H. polygyrus*-infected *Bhlhe40*$^{+/+}$, 6 *H. polygyrus*-infected *Bhlhe40*$^{-/-}$). **f**, Frequency of 7-AAD^{+} LPMs from *Bhlhe40*$^{+/+}$, *Bhlhe40*$^{-/-}$, *LysM-Cre*$^{-}$ *Bhlhe40*$^{fl/fl}$, and *LysM-Cre*$^{+}$ *Bhlhe40*$^{fl/fl}$ mice mock- or *H. polygyrus*-infected (pooled from 3 experiments, n=4 mock-infected *Bhlhe40*$^{+/+}$; 3 mock-infected *Bhlhe40*$^{-/-}$; 12 *H. polygyrus*-infected *Bhlhe40*$^{+/+}$ and *Bhlhe40*$^{-/-}$; 3 mock-infected *LysM-Cre*$^{-}$ *Bhlhe40*$^{fl/fl}$ and *LysM-Cre*$^{+}$ *Bhlhe40*$^{fl/fl}$; 11 *H. polygyrus*-infected *LysM-Cre*$^{-}$ *Bhlhe40*$^{fl/fl}$ and *LysM-Cre*$^{+}$

Bhlhe40$^{fl/fl}$). Data in **b-f** are mean ± s.e.m; each symbol represents an individual mouse (**b-d,f**). *$P \leq 0.05$; **$P < 0.01$; ***$P < 0.001$; ****$P < 0.0001$, unpaired two-sided Student's *t*-test.

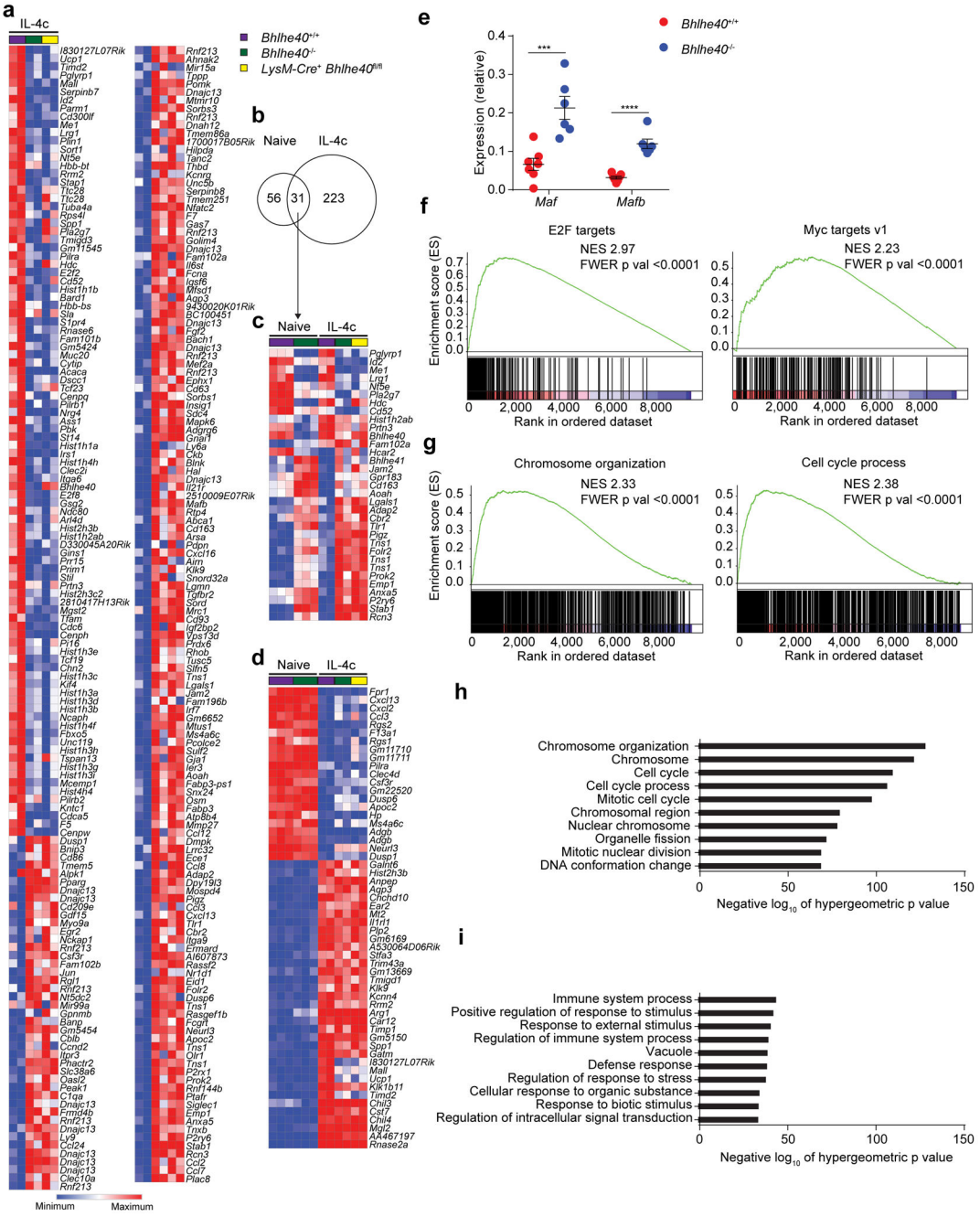

Figure 7. Bhlhe40 regulates gene expression to modulate proliferation, but not alternative activation, in LPMs during type 2 immunity.

a, Gene expression microarray data were analyzed for genes differentially expressed by ≥2-fold in LPMs from *Bhlhe40*$^{+/+}$, *Bhlhe40*$^{-/-}$, and *LysM-Cre*$^{+}$ *Bhlhe40*$^{fl/fl}$ mice treated with IL-4c. **b-d**, Gene expression microarray data were analyzed for shared and unique Bhlhe40-dependent genes (≥2-fold differentially expressed, depicted as a Venn diagram) (**b**), shared Bhlhe40-dependent genes (**c**), and expression of the LPM alternative activation signature (**d**) in LPMs from *Bhlhe40*$^{+/+}$, *Bhlhe40*$^{-/-}$, and *LysM-Cre*$^{+}$ *Bhlhe40*$^{fl/fl}$ mice unstimulated or treated with IL-4c. **e**, qRT-PCR of *Maf* and *Mafb* expression relative to *Hprt* in *Bhlhe40*$^{+/+}$

and *Bhlhe40*$^{-/-}$ LPMs from mice treated with IL-4c (pooled from 3 experiments, n=7 *Bhlhe40*$^{+/+}$, 6 *Bhlhe40*$^{-/-}$). **f,g**, GSEA of gene expression microarray data for representative Hallmark (**f**) and C5 gene sets (**g**) enriched in *Bhlhe40*$^{+/+}$ vs. *Bhlhe40*$^{-/-}$ LPMs from IL-4c-treated mice. NES, normalized enrichment score. FWER, family-wise error rate. **h,i**, MSigDB C5 gene set enrichment was analyzed using the lists of genes expressed at ≥1.5-fold in *Bhlhe40*$^{+/+}$ vs. *Bhlhe40*$^{-/-}$ (**h**) or *Bhlhe40*$^{-/-}$ vs. *Bhlhe40*$^{+/+}$ LPMs from IL-4c-treated mice (**i**). Microarray data from naïve LPMs (n=3/group, reanalyzed from Fig. 3) and *in vivo* IL-4c-stimulated LPMs (n=2/group) are from single separate experiments. Data in **e** are mean ± s.e.m; each symbol represents an individual mouse (**e**). ***$P < 0.001$; ****$P < 0.0001$, (**e**) unpaired two-sided Student's *t*-test, (**f,g**) NES and FWER, and (**h,i**) one-sided hypergeometric test.

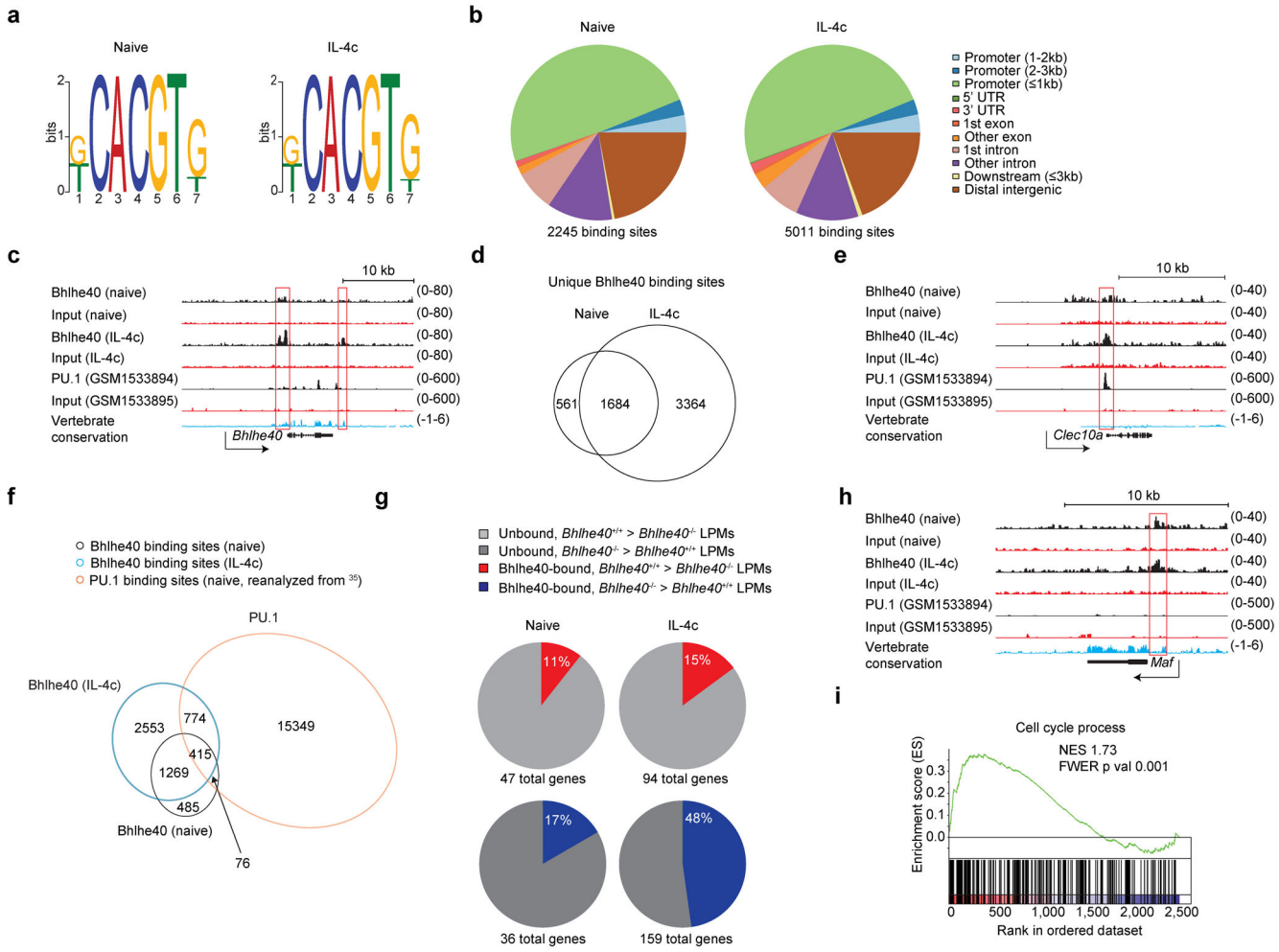

Figure 8. Bhlhe40 directly regulates gene expression in LPMs in an activation state-dependent manner.

a, Bhlhe40 ChIP-seq data were analyzed for consensus binding motifs in LPMs from naive (left) and IL-4c-treated mice (right). **b**, Bhlhe40 ChIP-seq data were analyzed for locations of Bhlhe40 peaks in the genome in LPMs from naive (left) and IL-4c-treated mice (right). UTR, untranslated region. **c**, Tracings of Bhlhe40 binding, PU.1 binding, and vertebrate conservation at the *Bhlhe40* locus. **d**, Bhlhe40 ChIP-seq data were analyzed for shared and unique Bhlhe40 binding sites in LPMs from naive and IL-4c-treated mice (depicted as a Venn diagram). **e**, Tracings of Bhlhe40 binding, PU.1 binding, and vertebrate conservation at the *Clec10a* locus. **f**, Naïve LPM Bhlhe40 ChIP-seq data, *in vivo* IL-4c-stimulated LPM Bhlhe40 ChIP-seq data, and naïve LPM PU.1 ChIP-seq data were analyzed for shared and unique Bhlhe40 and PU.1-bound genes between the three samples (depicted as a Venn diagram). **g**, The proportion of Bhlhe40-bound, Bhlhe40-dependent genes (≥2-fold differentially expressed in *Bhlhe40*$^{+/+}$ and *Bhlhe40*$^{-/-}$ LPMs) in LPMs from naïve mice and Bhlhe40-bound, Bhlhe40-dependent genes (≥2-fold differentially expressed in *Bhlhe40*$^{+/+}$ and *Bhlhe40*$^{-/-}$ LPMs) in LPMs from IL-4c-treated mice. **h**, Tracings of Bhlhe40 binding, PU.1 binding, and vertebrate conservation at the *Maf* locus. **i**, GSEA of gene expression microarray data for Bhlhe40-bound genes from LPMs from *Bhlhe40*$^{+/+}$ and *Bhlhe40*$^{-/-}$

mice treated with IL-4c for the C5 Cell Cycle Process gene set. NES, normalized enrichment score. FWER, family-wise error rate. LPM Bhlhe40 ChIP-seq data (n=1/group) and microarray data from *in vivo* IL-4c-stimulated LPMs (n=2/group) are from single separate experiments. LPM PU.1 ChIP-seq data reanalyzed from[35]. (**i**) NES and FWER.